3D IMAGING OF THE ENVIRONMENT

Mapping and Monitoring

Edited by
John Meneely

CRC Press
Taylor & Francis Group

3D Imaging of the Environment

This is a comprehensive, overarching, interdisciplinary book and a valuable contribution to a unified view of visualisation, imaging, and mapping. It covers a variety of modern techniques, across an array of spatial scales, with examples of how to map, monitor, and visualise the world in which we live. The authors give detailed explanations of the techniques used to map and monitor the built and natural environment and how that data, collected from a wide range of scales and cost options, is translated into an image or visual experience. It is written in a way that successfully reaches technical, professional, and academic readers alike, particularly geographers, architects, geologists, and planners.

FEATURES

- Includes in-depth discussion on 3D image processing and modeling
- Focuses on the 3D application of remote sensing, including LiDAR and digital photography acquired by UAS and terrestrial techniques
- Introduces a broad range of data collection techniques and visualisation methods
- Includes contributions from outstanding experts and interdisciplinary teams involved in earth sciences
- Presents an open access chapter about the EU-funded CHERISH Project, detailing the development of a toolkit for the 3D documentation and analysis of the combined coastline shared between Ireland and Wales

Intended for those with a background in the technology involved with imaging and mapping, the contributions shared in this book introduce readers to new and emerging 3D imaging tools and programs.

3D Imaging of the Environment

Mapping and Monitoring

Edited by John Meneely

CRC Press
Taylor & Francis Group
Boca Raton London New York

CRC Press is an imprint of the
Taylor & Francis Group, an informa business

Designed cover image: © Historic Environment Scotland, The Engine Shed, Stirling, Scotland

First edition published 2024
by CRC Press
2385 NW Executive Center Drive, Suite 320, Boca Raton FL 33431

and by CRC Press
4 Park Square, Milton Park, Abingdon, Oxon, OX14 4RN

CRC Press is an imprint of Taylor & Francis Group, LLC

ISBN: 978-0-367-33793-3 (hbk)
ISBN: 978-1-032-10895-7 (pbk)
ISBN: 978-0-429-32757-5 (ebk)

DOI: 10.1201/9780429327575

Typeset in Times
by Apex CoVantage, LLC

Contents

Preface

The field of 3D imaging has undergone a remarkable transformation over the past few decades, fuelled primarily by the emergence of new technologies, the growing demand for realistic, immersive visual experiences and the ability to easily share the results online.

This text is an essential guide for anyone interested in learning about this exciting field. Whether you are a student, a researcher, or a professional, this book provides a wide-ranging overview of the techniques, technology, and applications used today.

With contributions from leading specialists in the field, it covers an expansive range of topics and technologies over a vast range of scales, such as photogrammetry, laser scanning, drone mapping, and 3D printing. Through a collection of case studies, it explores the applications of 3D imaging in various fields, such as our built cultural heritage, geomorphology, archaeology, zoology, and climate change and how 3D technologies are being used to map, monitor, visualise, and share the research being carried out in these areas.

The text is designed to be accessible to a broad spectrum of readers, from beginners to advanced users, and includes many links to online 3D content of the examples covered. It provides a general introduction to the field of 3D imaging while also giving in-depth coverage of advanced 3D technologies and techniques.

I hope that this book will serve as a valuable resource for anyone interested in 3D imaging and that it will inspire new ideas and innovations in this exciting and rapidly evolving field.

John Meneely

Editor

John Meneely is the founder of 3D Surveying Ltd, having previously worked as Senior Research Technician at the School of Natural and Built Environment, Queen's University, Belfast. With over 30 years of experience in practical research, he has worked all over the world with interdisciplinary teams across the earth sciences. His expertise lies in using a variety of 3D laser scanning and other digital technologies to map, monitor, and visualise the built and natural environment across a wide range of spatial and temporal scales. He has presented his work at many national and international conferences and been the keynote speaker at several 3D digital technologies conferences. He was on the advisory board for SPAR Europe for two years – Europe's largest 3D scanning conference – and invited to speak at the 2009 International Council on Monuments and Sites (ICOMOS) symposium in Malta on the use of terrestrial laser scanning. His early research and publications focused on studying the catastrophic decay of building stone under complex environmental regimes and the digital documentation of natural and built heritage sites for several geological, geographical, archaeological, managerial, and educational applications. His recent interest has extended his data collection skills into 3D visualisation via 3D printing, VR, and AR. He is currently advising several SMEs, primarily in the environmental monitoring, built heritage, construction, and facilities management sector on integrating 3D technologies into their workflow.

Contributors

Kathryn Adamson
Department of Geography
Manchester Metropolitan University
Manchester, England, UK

Louise Barker
Department of Archaeology
Royal Commission on the Ancient and Historic Monuments of Wales (RCAHMW)
Shrewsbury, England, UK

Iestyn D. Barr
Department of Geography
Manchester Metropolitan University
Manchester, England, UK

James Barry
Geological Survey Ireland
Department of the Environment, Climate and Communications
Dublin, Ireland

Michela Bertolotto
School of Computer Science
University College
Dublin, Ireland

Marco Callieri
Visual Computing Laboratory
Institute of Information Science and Technologies
National Research Council of Italy
Pisa, Italy

Michael Casey
Dublin, Ireland

Paul Chapman
School of Simulation and Visualisation
Glasgow School of Art
Glasgow, Scotland, UK

Kendrew Colhoun Director
KRC Ecological Ltd
Newcastle, Northern Ireland, UK

Anthony Corns
The Discovery Programme
Dublin, Ireland

Kieran Craven
Geological Survey Ireland
Department of the Environment, Climate and Communications
Dublin, Ireland

Sean Cullen
Geological Survey Ireland
Department of the Environment, Climate and Communications
Dublin, Ireland

Sarah Davies
Department of Geography and Earth Sciences
Aberystwyth University
Aberystwyth, Wales, UK

Colm Donnelly
School of Natural and Built Environment
Queen's University
Belfast, Northern Ireland, UK

Toby Driver
Department of Archaeology
Royal Commission on the Ancient and Historic Monuments of Wales (RCAHMW)
Shrewsbury, England, UK

Trevor Fisher
Banbridge, Northern Ireland, UK

Adam Frost
Historic Environment Scotland
The Engine Shed
Stirling, Scotland, UK

Michal Gallay
Institute of Geography
Faculty of Science
Pavol Jozef Šafárik University
Košice, Slovakia

Tim Gomes
Idaho Virtualization Laboratory
Idaho Museum of Natural History
Idaho State University
Pocatello, Idaho, USA

Hywel Griffiths
Department of Geography and Earth Sciences
Aberystwyth University
Aberystwyth, Wales, UK

Harkin Aerial
Oyster Bay, New York, USA

Scott Harrigan
Virtual Surveyor
Raleigh, North Carolina, USA

Sandra Henry
The Discovery Programme
Dublin, Ireland

Zdenko Hochmuth
Institute of Geography
Faculty of Science
Pavol Jozef Šafárik University
Košice, Slovakia

Markus Hollaus
Research Group Photogrammetry
Department of Geodesy and Geoinformation
Vienna University of Technology (TU Wien)
Vienna, Austria

Daniel Hunt
Department of Archaeology
Royal Commission on the Ancient and Historic Monuments of Wales (RCAHMW)
Shrewsbury, England, UK

Benedikt Imbach
Aeroscout GmbH
Hochdorf, Switzerland

Stuart Jeffrey
School of Simulation and Visualisation
Glasgow School of Art
Glasgow, Scotland, UK

Sarah Kandrot
Department of Geography
University College Cork
Cork, Ireland

Ján Kaňuk
Institute of Geography
Faculty of Science
Pavol Jozef Šafárik University
Košice, Slovakia

Michael King
Newry, Mourne, and Down District Council
Downpatrick and Newry, Northern Ireland, UK

Debra Laefer
Tandon School of Engineering
New York University
Brooklyn, New York, USA

Timothy Lane
Department of Geography and Environmental Science
John Moores University
Liverpool, England, UK

Alan Lauder
Wildlife Conservation and Science Ltd
Kilcoole, Wicklow, Ireland

Ciaran Lavelle
National Museums Northern Ireland
Cultra, Northern Ireland, UK

Tony Martin
School of Natural and Built Environment
Queen's University
Belfast, Northern Ireland, UK

John Meneely
3D Surveying Ltd
Banbridge, Northern Ireland, UK

Aaron Miller
School of Natural and Built Environment
Queen's University
Belfast, Northern Ireland, UK

Daniel Moloney
Redcastle, Donegal, Ireland

Konstantin Nebel
Geography and Environmental Research Group
John Moores University
Liverpool, England, UK

Ulrich Ofterdinger
School of Natural and Built Environment
Queen's University
Belfast, Northern Ireland, UK

Edward Pollard
The Discovery Programme
Dublin, Ireland

Victor Portela
School of Simulation and Visualisation
Glasgow School of Art
Glasgow, Scotland, UK

Jesse Pruitt
Idaho Virtualization Laboratory
Idaho Museum of Natural History
Idaho State University
Pocatello, Idaho, USA

Patrick Robson
Department of Geography and Earth Sciences
Aberystwyth University
Aberystwyth, Wales, UK

Ján Šašak
Institute of Geography
Faculty of Science
Pavol Jozef Šafárik University
Košice, Slovakia

Robert Shaw
The Discovery Programme
Dublin, Ireland

Linda Shine
The Discovery Programme
Dublin, Ireland

Brian Sloan
School of Natural and Built Environment
Queen's University
Belfast, Northern Ireland, UK

Jozef Šupinský
Institute of Geography
Faculty of Science
Pavol Jozef Šafárik University
Košice, Slovakia

Leif Tapanila
Idaho Virtualization Laboratory
Idaho Museum of Natural History
Idaho State University
Pocatello, Idaho, USA

Willem G. M. van der Bilt
University of Bergen
Bergen, Norway

Evelyn Vollmer
Idaho Virtualization Laboratory
Idaho Museum of Natural History
Idaho State University
Pocatello, Idaho, USA

Anh Vu Vo
School of Computer Science
University College Dublin, Ireland

Stephen Weir
National Museums Northern Ireland
Cultra, Northern Ireland, UK

Lyn Wilson
Historic Environment Scotland
The Engine Shed
Stirling, Scotland, UK

Carlo Zgraggen
Aeroscout GmbH
Hochdorf, Switzerland

4 Laser Scanning of a Complex Cave System during Multiple Campaigns

A Case Study of the Domica Cave, Slovakia

Ján Kaňuk, Jozef Šupinský, John Meneely, Zdenko Hochmuth, Ján Šašak, Michal Gallay, and Marco Callieri

INTRODUCTION

Caves are natural sub-surface hollow forms with an extremely complex three-dimensional (3D) morphology in both horizontal and vertical directions. Their research provides valuable knowledge for geology, hydrology, geomorphology, biology, and also history. Caves have attracted people's attention since ancient times when prehistoric humans sought refuge from adverse weather and cold or wild animals and enemies. Today, the inherent mystery and natural beauty of caves captivate human curiosity, and many have become tourist attractions that can also lead to protection. From a scientific point of view, caves are an important source of information about past environments and are important for understanding contemporary conditions and changes. Past climates can be reconstructed from the preserved natural materials, such as sediments, ice, and geomorphological forms, but also from objects of human origin (e.g., bones, working tools, paintings, ash).

From a mapping perspective, caves are a major challenge due to the complexity of surface shapes, confined spaces, lack of light, and the abundance of water, mud, or even ice (Gallay et al., 2015). Traditionally, cave surveying was mostly carried out by volunteer caving clubs and associations and, to a lesser extent, by professional cavers employing mine surveying methods, such as tacheometry. Despite the immense effort of cave surveyors, the resulting maps are highly generalized 2D floor plans or projected vertical side views, with very little 3D information. Currently, mapping with a laser distance measurer, inclinometer, and compass is widely used. Tourist 'show caves'—which have been made accessible to the general public by

DOI: 10.1201/9780429327575-

guided visits—are usually mapped with a total station. These maps usually comprise a traverse, showing the course of the cave to which other measurements are connected—typically, the position of side corridors, passages, large speleothems, water streams, lakes, or abysses are only recorded, with little or no information on small-scale features.

Other technologies based on underground global navigation system (U-GPS) (Wenger, 2004), sonar (Stipanov et al., 2008), ground-penetrating radar (Chamberlain et al., 2000), seismic (Beres et al., 2001), or electric resistivity methods (Peterson and Berg, 2001) have previously been used to try and refine the mapping of caves.

However, these methods still are not extensively applied, principally for their complexity and demands on technical equipment and data processing. Recently, remote sensing technologies, such as close-range photogrammetry (Triantafyllou et al., 2019) and 3D laser scanning (Mohammed Oludare and Pradhan, 2016), or their combined use (Lerma et al., 2010) have become popular in cave mapping. These methods are capable of capturing an unprecedented level of detail and are faster than other methods used to date. Both these methods generate millions of 3D point measurements (usually referred to as point clouds), representing the mapped surface highly accurately in the order of millimeters and without the need to generate a surveying traverse. The application of close-range photogrammetry is, however, limited by suitable illumination usually requiring powerful artificial lights. In the case of laser scanning, which uses light detection and ranging technology (LiDAR), this darkness of caves is not a problem. For this reason, terrestrial laser scanners (TLS) have been increasingly used in mapping caves despite its relatively high cost when compared to digital cameras and lights needed for photogrammetry.

A distinction has to be made between TLS and mobile laser scanning (MLS). TLS is performed from static ground-based platforms, usually placed on a tripod, with a laser scanner rotating around its axis. It records the horizontal and vertical angle of the emitted laser beam, the time it takes that beam to return from a surface to the scanner, plus how much of that emitted beam returned, and it can do this millions of times per second. From this it can calculate a x,y,z coordinate, relative to the scanner and assign an intensity value (I) to each point calculated from the return strength of the laser from a surface.

Once a single scan is complete, it has to be moved to another location to capture the entire scene without data shadows during mapping. The individual point cloud collected from each scanning position is then registered (joined together) to generate a single point cloud in a common coordinate system.

In order for the registration to be accurate and successful, a sufficient portion of successive scans must overlap. This registration of the data is performed in dedicated, usually vendor-specific software, either manually or automatically. In recent years, a significant trend in TLS is the transfer of completed scans via a Wi-Fi or Bluetooth to a laptop or dedicated tablet for instant, in-field registration. This has many advantages in cave mapping—primarily the ability to ensure that no areas have been missed before leaving a difficult to access area.

The principle of MLS is based on the recordings of two synchronized devices: the inertial measurement unit (IMU) and the laser scanner. The IMU records the orientation angles along the x, y, z axes in 3D space to determine the trajectory of the laser scanner. The coordinates of the individual points recorded by the laser scanner are then calculated based on the laser triangulation (pulse emission angle and distance) with respect to the position of the scanner. The main benefit of MLS is in the speed of mapping and reduced data shadows by the continual movement of the scanner in space, providing an opportunity to scan around any object. On the other hand, the limited ability to record the trajectory of the scanner's motion using the IMU compromises the accuracy of the 3D coordinates of the resulting point cloud. IMU locates itself by employing various sensors, such as a gyroscope, accelerometer, compass, barometer, and sometimes GNSS. The basic problem is that the frequency of recordings by IMU is over 1,000 times lower compared to the frequency of laser scanning. These shortcomings in tracking the scanner motion must be compensated for by calculations, for example, using the simultaneous location and mapping (SLAM) method. This method is becoming widely used in MLS.

TLS is often preferred over MLS for its higher positional accuracy and high spatial density of recorded points in mapping complex cave morphologies (Mohammed Oludare and Pradhan, 2016). Although there is a wide range of less costly surveying methods, LiDAR has the potential to replace traditional techniques for cave mapping. The capabilities of TLS in cave mapping are demonstrated in this chapter by showing the results from mapping over 5,000 m underground of the World Heritage Site Domica Cave in Slovakia.

REVIEW OF THE PUBLISHED WORKS ON LASER SCANNING IN CAVES

The application of laser scanning in caves dates back to the late 1980s and only focused on renowned sites, such as Altamira in northern Spain between 1988 and 2001 (Donelan, 2002) or Cosquer Cave in France in 1994 (Thibault, 2001), which were mapped by short-range (2 m), time-consuming and laborious active triangulation scanners. Today, this scanning approach is predominantly used for high-detail 3D scanning of small objects, using commercially available devices such as Kinect (Hämmerle et al., 2014) or the FARO Freestyle™.

Even after more than 30 years since the first TLS in caves, few cave systems are mapped in a large scale. An overview of works focused on mapping caves using TLS is presented in Gallay et al. (2015) or Mohammed Oludare and Pradhan (2016). A large number of cave laser scanning projects remain unpublished or published in local magazines making them difficult to find.

Table 4.1 presents a chronological overview of publications demonstrating the use of TLS in various caves, the reason for mapping, the length of the mapped parts, and the scanning equipment used. This list is by no means a complete overview. The simple analysis of the number of scientific papers in the Scopus database by using the query (TITLE-ABS-KEY (lidar AND cave)) OR (TITLE-ABS-KEY (laser AND scanning AND cave)) found 282 documents published since 1995. This indicates the growth in the use of laser scanning to survey caves has intensified since 2008 from about 5 up to 30 publications per year in 2020.

The review in Table 4.1 suggests that, before 2010, laser scanning of caves was performed mainly for archaeological research in small but significant sites where

TABLE 4.1
Summary of Published Works Concerning Laser Scanning in Caves

Year	Author	Location	Country	Purpose of Laser Scanning Mission	Range	Type of Scanner Device
1999	Perperidoy et al. (2010)	Chapel's Cave	USA	Documentation	Unknown	Unknown
2001	Thibault	Cosquer Cave (1994)	France	Archeology	Unknown	SOISIC
2001	Robson-Brown et al.	Dordogne Caves	France	Archeology	2 scans (wall)	Surveyor ALS
2002	Donelan	Altamira Cave	Spain	Archeology	Unknown	Minolta VI-700
2003	Caprioli et al.	Castellane Grotte Cave	Italy	Archeology	100 m	Mensi-GS100
2003	Westerman et al.	Peak Cavern Vestibule	UK	Archeology	Unknown	RIEGL LMS-Z360
	El-Hakim et al.	Baiame Cave	Australia	Archeology	Unknown	RIEGL LMS-Z210i
2004	The Courier (Channel 4 Time team)	Wemyss Caves	Scotland	Archeology	Unknown	Unknown
2005	Aujoulat	Veilmouly Cave (1994)	France	Archeology	Unknown	SOISIC
2005	Fryer et al.	Baiame Cave	Australia	Archeology	Unknown	RIEGL LMS-Z210i
2005	Murphy et al.	Gaping Gill Cave	UK	Documentation	Unknown	RIEGL LMS-Z210i
2006	Beraldin et al.	Grotta dei Cervi	Italy	Archeology	Unknown	Big Scan prototype
2006	Doering et al.	Preacher's Cave	Bahamas	Archeology	20 m	Leica HDS 3000
2007	Tsakiri et al.	Kefala Cave	Greece	Documentation	Unknown	iQsun 880HE80
2008	Brich et al.	High Pesture Cave	UK	Documentation	Unknown	Trimble GS200
2008	Canavese et al.	Naica Cave	Mexico	Geology	110 m	FARO CAM2 Focus 3D
2009	Buchroithner & Geiseckner	Dachstein Southface Cave	Austria	Documentation	100 m	RIEGL LMS-Z420i
2009	Gonzalez-Aguilera et al.	Las Caldas, Pena de Candamo Caves	Spain	Archeology	Unknown	Trimble GS200
2009	Chandelier & Roche	Tautavel Cave	France	Paleontology	Unknown	Trimble GS200
2009	Pucci & Marambio	Olerdola Cave	Spain	Archeology	Unknown	RIEGL LMS-Z420

(Conitnued)

TABLE 4.1 *(Continued)*
Summary of Published Works Concerning Laser Scanning in Caves

Year	Author	Location	Country	Purpose of Laser Scanning Mission	Range	Type of Scanner Device
2009	Rüther et al.	Wonderwerk Cave	South Africa	Archeology	Unknown	Leica HDS3000
2010	Grussenmeyer et al.	Les Fraux Cave	France	Archeology	Unknown	FARO Photon 120
2010	Lerma et al.	La Cova del Parpallo Cave	Spain	Archeology	Unknown	FARO LS 880HE
2010	McIntire	Mushpot Cave	USA	Documentation	150 m	Leica HDS6000
2011	Addison	Mammoth Cave	USA		4 000 m	
2011	Buchroithner	Eisriesenwelt Cave	Austria	Cryomorphology	1 000 m	FARO Photon 120/20 (2011); FARO Focus 3D (2013)
2011	Canavese et al.	Santa Barbara Cave System	Italy	Geomorphology	740 m	Leica HDS6100 and RIEGL LMS-Z210
2011	Jaillet et al.	Orgnac's Cave	France	Documentation	Unknown	Leica HDS 6000
2011	Petters et al.	Eisriesenwelt Cave	Austria	Cryomorphology	1 000 m	FARO Photon 120
2011	Roncat et al.	Marchenhohle Cave	Austria	Morphogenetic	150 m	Z+F Imager 5006i
2012	Azmy et al.	Gua Kelawar Cave	Malaysia	Zoology	14 scans	FARO Photon 120
2012	Buchroithner	Niah Caves	Malaysia	Documentation	Unknown	FARO Focus 3D
2012	Gašinec	Dobšinská Ice Cave	Slovakia	Cryomorphology	Unknown	Leica ScanStation C10
2012	Kordić et al.	Kuca Cave	Croatia	Archeology	Unknown	FARO Photon 120
2012	Lyons-Baral	Coronado Cave	USA	Hazards evaluation	200 m	Leica ScanStation C10
2012	Milius & Petters	Eisriesenwelt Cave	Austria	Cryomorphology	1 000 m	FARO Photon 120
2012	Santos Delgado et al.	El Sidrón Cave	Spain	Paleontology	50 m	Leica ScanStation C10
2013	Canevese and Tedeschi	Re Tiberio Cave	Italy	Documentation	60 m	Leica HDS6100

TABLE 4.1 ***(Continued)***
Summary of Published Works Concerning Laser Scanning in Caves

Year	Author	Location	Country	Purpose of Laser Scanning Mission	Range	Type of Scanner Device
2013	Gede et al.	Pálvölgy Cave	Hungary	Documentation	Unknown	FARO Focus 3D, Leica ScanStation C10
2013	Lindgren & Galeazzi	Las Cuevas Cave	Belize	Documentation	Unknown	FARO Focus 3D
2013	McFarlane et al.	Gomatong Caves	Malaysia	Documentation	1 000 m	FARO Focus 3D
2013	Nash & Beardsley	Cathole Cave	Wales	Documentation	Unknown	Leica HDS6000
2013	Núñez et al.	Can Sadurní Cave	Spain	Archeology	Unknown	RIEGL LMS-Z420i
2013	Plan et al.	Mammuthöhle Cave	Austria	Geomorphology	200 m	Z+F Imager 5006i
2013	Puchol et al.	Pastora Cave	Spain	Archeology	Unknown	FARO Photon 120
2013	Silvestre et al.	Algar do Penico Cave	Portugal	Documentation	80 m	Leica ScanStation C10
2013	Yumin	Lianhua Cave,Tianlongshan Cave	China	Archeology	Unknown	Unknown
2014	Berenguer-Sempere et al.	Castil Ice Cave	Spain	Cryomorphology	72 m	Leica ScanStation C10
2014	Burens et al.	Les Fraux Cave	France	Archeology	430 m	FARO Photon 120, FARO Focus 3D
2014	Cosso et al.	Arma Pollera Cave	Italy	Documentation	Unknown	Z+F Imager 5010
2014	Hämmerle et al.	Dechen Cave	Germany	Comparsion	Unknown	RIEGL VZ-400, Kinect
2014	Hobléa et al.	Orgnac's Cave,Chauvet Cave	France	Documentation	Unknown	Leica HDS 6000
2014	Hoffmeister	Sodmein Cave	Egypt	Archeology	Unknown	RIEGL LMS-Z420i
2014	Kukutsch et al.	Amatérska Cave	Czechia	Documentation	1 300 m	Leica ScanStation C10

(*Conitnued*)

TABLE 4.1 *(Continued)*
Summary of Published Works Concerning Laser Scanning in Caves

Year	Author	Location	Country	Purpose of Laser Scanning Mission	Range	Type of Scanner Device
2014	Leonov et al.	Denisova Cave	Russia	Documentation	37 scans	FARO Focus 3D
2014	Novaković	Škocjan Caves	Slovenia	Documentation	Unknown	Leica ScanStation C10
2014	Tyree	Skoteino Cave	Greece	Documentation	Unknown	RIEGL LMS-Z420i
2014	Zlot & Bosse	Jenolan Caves	Australia	Documentation	17 100 m	Hannibal, Zebedee
2015	Bella et al.	Dupnica Cave	Slovakia	Geology	Unknown	Leica ScanStation C10
2015	Gallay et al.	Domica Cave	Slovakia	Geomorphology	1 600 m	FARO Focus 3D
2015	Marisco et al.	Santa Croce Cave	Italy	Documentation	90 m	Leica HDS 3000
2015	McFarlane et al.	Gomantong Caves	Malaysia	Zoology	1 000 m	FARO Focus 3D
2015	Santagata et al.	Grotta della lucerna Cave	Italy	Documentation	Unknown	Leica HDS 7000
2016	Hoffmeister	Ardelas Cave	Spain	Documentation	Unknown	RIEGL LMS-Z420i
2016	Kruger et al.	Rising Star Cave	South Africa	Archeology	Unknown	FARO Focus 3D
2016	Tyszkowski et al.	20 Caves	Poland	Documentation	Unknown	RIEGL VZ-400
2016	Yakar et al.	"Hadim" Cave	Turkey	Documentation	13 scans	OPTECH ILRIS
2017	Basantes et al.	Elviandi Cave	Ecuador	Documentation	450 m	FARO Focus 3D
2017	Citton et al.	Grotta della Básura Cave	Italy	Paleonthology	Unknown	Leica ScanStation 2
2017	Fabbri et al.	Grotta A Cave	Italy	Geology	Unknown	FARO CAM2 Focus 3D
2017	Pukanska et al.	Belianska Cave	Slovakia	Documentation	Unknown	Leica ScanStation C10
2018	De Waele et al.	Ca'Castellina Cave	Italy	Geomorphology	Unknown	FARO CAM2 Focus 3D
2018	Gómez-Lende & Sánchez-Fernández	Picos de Europa Ice Caves	Spain	Cryomorphology	Unknown	Leica ScanStation C10, FARO Focus 3D

TABLE 4.1 *(Continued)*
Summary of Published Works Concerning Laser Scanning in Caves

Year	Author	Location	Country	Purpose of Laser Scanning Mission	Range	Type of Scanner Device
2018	Petrović et al.	Pećura and Zamna Caves	Serbia	Documentation	Unknown	Leica Nova MS50
2019	Aiello et al.	Grotta dei Pipistrelli	Italy	Documentation	72 scans	FARO Focus S70
2019	Kregar et al.	Kumik Cave	Slovenia	Documentation	2 000 m	Leica BLK360
2019	Nocerino et al.	Grotta Giusti	Italy	Documentation	Unknown	Leica HDS7000
2019	Radicioni et al.	Frasassi Caves	Italy	Documentation	Unknown	FARO Focus 3D
2019	Shults et al.	Kyiv Pechersk Lavra Caves	Ukraine	Documentation	Unknown	Leica ScanStation
2019	Sorrioux et al.	Gouffre Georges	France	Geology	250 m	RIEGL VZ-1000
2019	Šupinský et al.	Silická ľadnica Cave	Slovakia	Cryomorphology	50 m	RIEGL VZ-1000
2019	Šupinský et al.	Domica Cave	Slovakia	Documentation	6 000 m	FARO Focus 3D, RIEGL VZ-1000
2019	Zeid et al.	Fumane Cave	Italy	Archeology	Unknown	Leica ScanStation C10

a small number of scan positions was sufficient (up to 10) (Robson-Brown et al., 2001; Westerman et al., 2003; González-Aguilera et al., 2009). Since 2010, laser scanning has been applied on a larger scale. The variety of scanners on the market and improved capabilities, lower price, and new methods of processing point clouds stimulated the application also in caves. Gradually, longer parts of caves were mapped, and larger areas of caves with a larger number of scanning positions were performed. The main purpose was in cave documentation (Petters et al., 2011; Kuda et al., 2014; Zlot and Bosse, 2014; Kregar et al., 2019) and geomorphological analysis (Roncat et al., 2011; Buchroithner et al., 2012; Bella et al., 2015; Fabbri et al., 2017; Gallay et al., 2016). Other applications include, for example, analysis of cryomorphological characteristics of cave ice (Gašinec et al., 2012; Gómez-Lende and Sánchez-Fernández, 2018), as well as evaluation of the volume change of glacial glaze (Milius and Petters, 2012; Šupinský et al., 2019). TLS in caves was also used in zoology for animal counting purposes, in assessing potential natural risks, and in paleontology (Azmy et al., 2012; Lyons-Baral, 2012; Citton et al., 2017).

There are two main types of TLS technology. The most widely used scanners are based on emitting pulses of laser energy (time-of-flight scanners), which reach a longer range than the second type based on continuous emission of laser energy (continuous wave (CW), phase-based scanners). In narrow passages, however, t advantage of pulse-based laser scanners cannot be fully exploited. The deplo devices comprise pulse-based scanners RIEGL LMS/VZ Series™ (Núñez et a 2013; Tyszkowski et al., 2016; Šupinský et al., 2019), Leica ScanStation (Pukan et al., 2017; Gómez-Lende and Sánchez-Fernández, 2018; Zeid et al., 2019), Le BLK™ Series (Kregar et al., 2019); or phase-based scanners FARO Focus 3D X Series™ (Gallay et al., 2015; Aiello et al., 2019; Radicioni et al., 2019), Le HDS™ Series (Marsico et al., 2015; Santagata et al., 2015; Nocerino et al., 20 and Z+F IMAGER™ (Roncat et al., 2011; Plan et al., 2013; Cosso et al., 2014). T list of reviewed works supports that TLS in caves is possible even in challeng conditions (Buchroithner and Gaisecker, 2009). In addition, MLS brings new po sibilities for cave mapping (Bosse et al., 2012; Zlot and Bosse, 2014; Kaul et a 2016).

LASER SCANNING OF THE DOMICA CAVE

This case study concerns laser scanning of the Domica Cave and some of its exte surface surroundings. The resulting geodatabase allows for the creation of deta and accurate maps, cross-sections, and plan views and also extends geomorpholo cal, climatological, speleo-biological, and hydrological research of the cave. TL has been carried out on the cave system from 2014. First, the show cave part w scanned (ca. 1,500 m), and then other publicly unavailable parts followed. In 2014, a airborne laser scanning (ALS) campaign was carried out to map the surface.

Geographical Setting

Domica Cave is located in the Triassic limestones of the Slovak Karst Mounta in southeastern Slovakia, about 1 km west of the border with Hungary (Figure 4. The cave is part of a much longer system continuing through the state border into th Aggtelek Karst, where it is called Baradla Cave. The Domica-Baradla Cave syste has a total length of 27,476 m (Gaál and Gruber, 2014). The Slovakian (Domica) se tion has a length of 8,014 m. It is a unique cave with colorful flowstone decorat characterized by cascading lakes, typical onion-shaped stalactites, flowstone dru shields, and stegamites. The uniqueness of the cave is also emphasized by spec fauna and flora. For these reasons, the cave is a listed UNESCO World Natu Heritage Site and a Ramsar Site. The detailed characteristics of the entire Domi Baradla Cave system can be found in Gaál and Gruber (2014).

The cave was formed by underground streams, two of which still flow thro the system: the Domický stream and the Styx river, which continues into th Hungarian section. Domica Cave is regularly affected by floods in winter. The floods have a destructive effect on the decoration of the cave as well as on the infr structure, especially in the publicly accessible areas. The presence of tourists h also induced anthropogenic interventions in the cave such as building water da and pavements. A better understanding of the reoccurring floods were one of th rationales behind the application of TLS and ALS to generate a detailed 'digi twin' of this system.

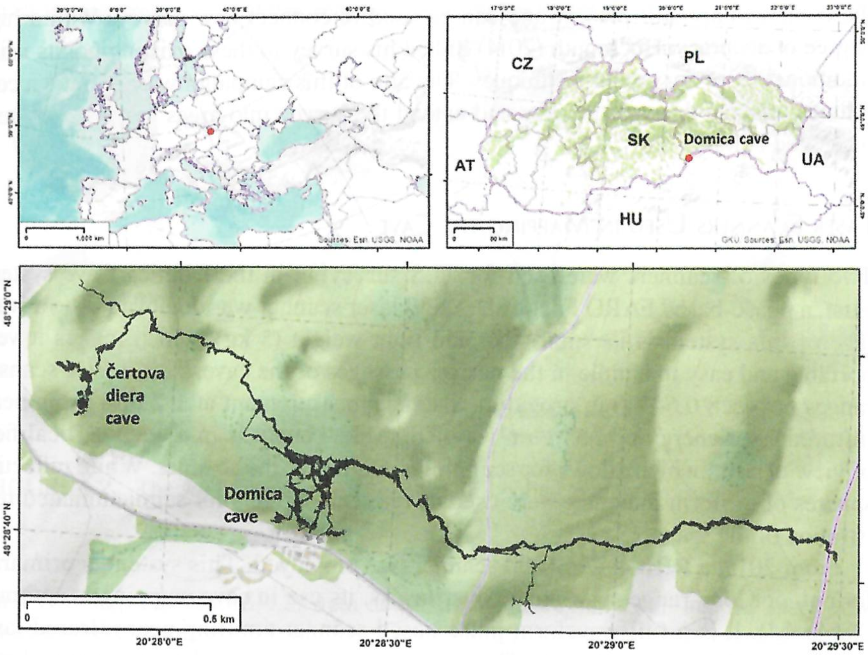

FIGURE 4.1 Location of the Domica cave system including the Devil's Hole Cave (Čertova diera) overlayed with shaded airborne LiDAR digital terrain model and land cover map.

Source: © Open Street Map

Domica Cave has been mapped several times since its discovery in 1932 by a soldier, Ján Majko. Traditionally mine-surveying methods and equipment were used for mapping. Just after the discovery, the first comprehensive mapping of Domica was supervised by mining surveyor Paloncy. The aim of this survey was to generate a map of the new cave in the territory of former Czechoslovakia. At that time, the cave contained prehistoric artifacts untouched since the Neolithic people left the cave—thought to be due to the collapse of the entrance over 5,000 years ago. In 1937, Roth carried out a much more detailed mapping exercise, which focused on large halls rich in cave decoration. This produced a detailed map of selected parts of the cave at a scale of 1:100.

The purpose of surveying the cave in 1949 was in locating and establishing the underground state border between Slovakia and Hungary. The mission resulted in a highly accurate and well-stabilized surveying network with detailed recording of the measurements. In 1964, a map created by Droppa and Chovan was published (Droppa 1964), complementing the 1949 cave floor plan with side elevations. Further mapping by Droppa (1972) recorded the ground levels of the cave passages, and this indicated a gradual erosion of the cave base during its formation. The successive opening of new parts of the cave led to greater invasive interventions. In order to build an artificial tunnel from Suchá chodba to the Panenská chodba passage, a detailed mine survey was carried out in 1975 (Novoveský, 1975). The surveying points used in all these surveys are still present and can be used to connect new surveys with a high degree of accuracy. Hochmuth (2014) linked his survey to these existing points using traditional mine-surveying techniques. The aim of this campaign was to make a continuous traverse through the cave and extend the survey into areas that had not been measured before.

Laser Scanners Used in Mapping the Cave

Two types of scanners were used for TLS surveying in the Domica Cave system. First, a phase-based FARO Focus 3D X 130 laser scanner was deployed. The advantage of this system is its small size and light weight (5 kg), which makes it very portable and easy to handle in the narrow passages of the cave. This device scans at ranges between 0.6–130 m providing distance measurement at ± 2 mm using near-infrared laser energy of 1,550 nm wavelength. Its benefit is in a wide vertical field of view of 310°, which allows for scanning areas above the scanner. White reflective spheres of uniform diameter were used as reference targets for semiautomated registration of the scans.

From 2015, a RIEGL VZ-1000 scanner was employed. This system is primarily for outdoor long-range surveying, nevertheless, its use in cave mapping is common (Table 4.1). It is a full waveform pulse-based scanner emitting near-infrared laser pulses of 1,550 nm wavelength. The measurement precision along the range direction is ± 3 mm with a minimal scanning range from 1.5 m to 1,400 m. Compared to the FARO scanner, the VZ-1000 is relatively heavy (10 kg with batteries), which made it difficult to handle in the cave. The most significant drawback of this scanner in caves is the limited vertical angle of 100°, which complicates capturing data on the ceiling directly above the scanner. The data shadows created with this system have to be reduced by closer placement of scanning positions to each other or scanning the ceiling by tilting the scanner.

Besides the distance between consecutive scanning positions, the density of point measurements is controlled by the frequency of measurements. The RIEGL VZ-1000 is capable of emitting 550,000 pulses per second (550 kHz pulse repetition rate). Scanning at this rate takes approximately 80 seconds with a scanning detail of 0.06° in the vertical and horizontal directions. The measurement frequency of the FARO Focus 3D X 130 is up to 950,000 points per second and at resolution ¼ (0.036°), scanning from one position takes approximately 3 minutes and 26 seconds, although this time can be increased to improve the quality of the data. The VZ-1000 is capable of recording an unlimited number of pulse echoes. Practically, only echoes above a set quality threshold are recorded, and they can be further filtered based on pulse waveform deviation or rescaled intensity. This information can be used to remove stray points.

The Workflow of LiDAR Cave Mapping

The TLS data acquisition is followed by several steps of data processing. The main steps of the workflow to generate a cave map are shown in Figure 4.2. The first task is the registration of individual scans acquired from each scanning location. The

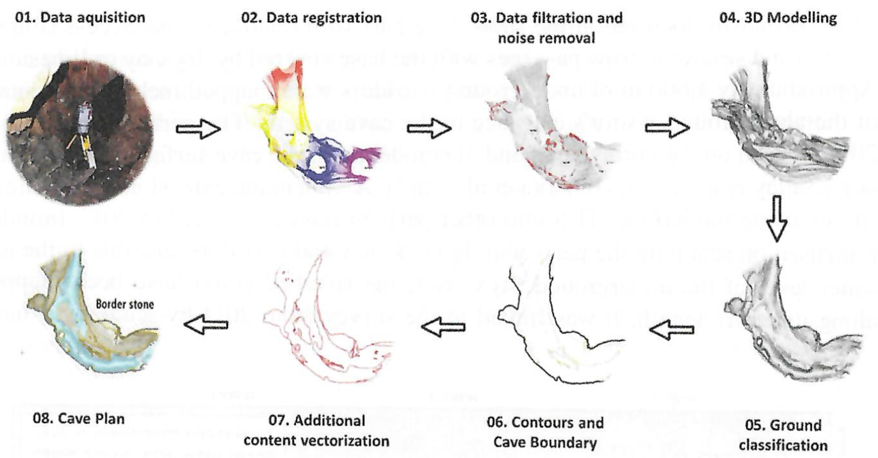

FIGURE 4.2 The workflow of converting the TLS point cloud into a cave map.

first two steps in Figure 4.2, data acquisition and registration, are the most time-consuming. Scanning positions need to be carefully chosen to keep their number reasonably low but, at the same time, minimize data shadows while still ensuring a sufficient overlap with the previous scan. Ultimately, a carefully planned TLS survey allows for the application of automated registration procedures for adjusting the scan positions, resulting in minimized registration errors, typically in the order of millimetres. Gallay et al. (2015) explain the details of the TLS methodology of scanning in 2014 and Šupinský et al. (2019) describe the following TLS campaigns.

After the scans are registered into a single point cloud, it is necessary to filter out erroneous data (Kaňuk et al., 2019). These are mainly stray points form laser reflections with water or points with a high position of uncertainty due to low surface reflectivity. Point filtering and the denoising process are prerequisites for deriving any complex and realistic 3D surface models.

The Multifold Cave Laser Scanning Campaign

Data collection with a TLS was carried out in 43 separate surveys, totaling 178 scanning hours. From a practical point of view, the most time-consuming factor was ensuring the safe transport of the surveying equipment to a location and the stabilization of the device in very narrow passages in areas with water and mud. To date, this mapping has involved 1,029 scan locations with the RIEGL VZ-1000 and 786 positions with the FARO Focus 3D, generating an average of 9 million points per position. A typical day involved 4–8 hours of scanning underground, 46 scan locations with a spacing ranging from 2 to 20 m to ensure sufficient scan overlap. This achieved a point density ranging from 26,000 points.m^{-2} in large domes to 46,000 points.m^{-2} in narrow passages.

The first phase of mapping was performed in March 2014 with the FARO Focus 3D scanner (Gallay et al., 2015). This involved 327 positions during a 5-day campaign which primarily focused on the show cave part with relatively easy access (F 4.3 (C)) and several narrow passages with the base covered by dry clay or limes Approximately 1,600 m of underground corridors were mapped including a se of the aboveground visitor's entrance to the cave system. The period from 20 2017 focused on data processing and 3D modeling of the cave surface from thi vey (Gallay et al., 2016; Hofierka et al., 2017). A systematic extension of this survey using the RIEGL TLS into other parts of the cave started in 2017. Ini it focused on scanning the parts with large domes and corridors, and due to th water level of the underground Styx river, the riverbed could have been m along its entire length. It was linked to the survey from 2014 by scanning a

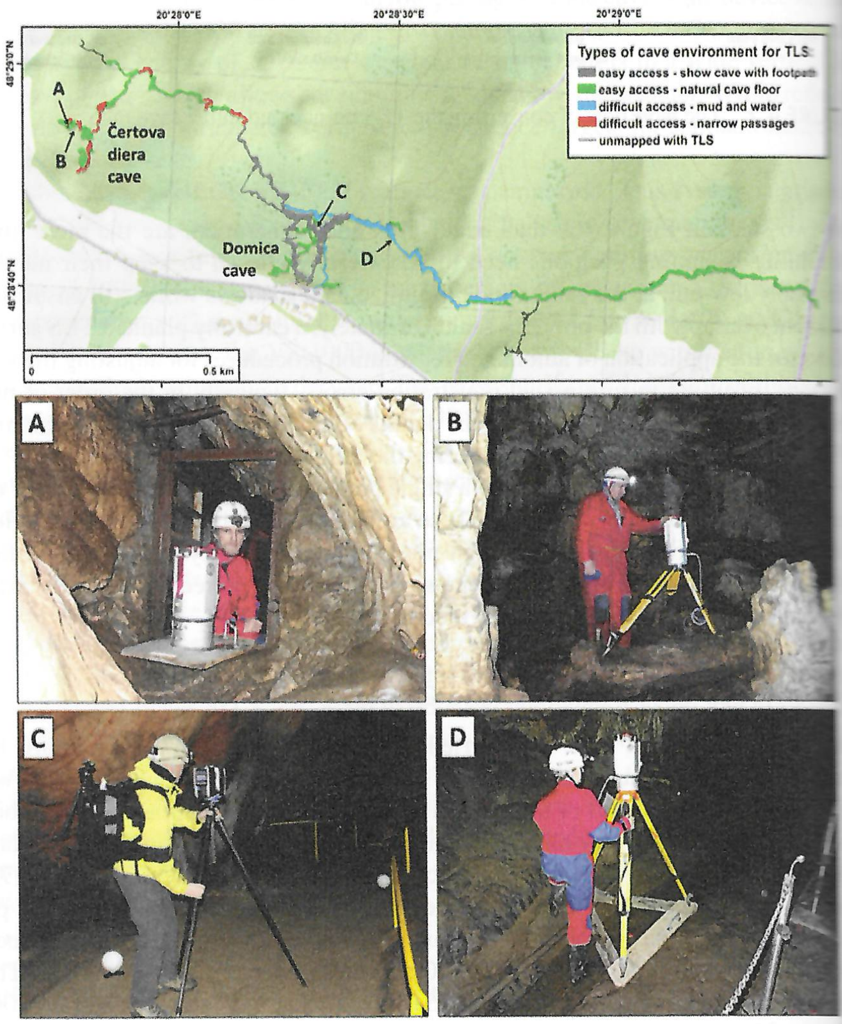

FIGURE 4.3 Various kinds of environmental conditions while laser scanning the D Cave are annotated with letters (A–D) and located on the map.

overlapping area that contained an artificial dam. There was no water present at the time of this survey, but the bottom of the riverbed was covered by mud. To prevent the scanner from sinking into this mud, a platform was made from wooden boards, which stabilized it during data collection (Figure 4.3 (D)). This allowed sections of the cave right up to the border with Hungary to be surveyed.

In 2018, the TLS mapping focused mainly on the Čertova diera Cave (Devil's Hole). This part of the system is characterized by alternating spacious domes and narrow passages in which one has to crawl to pass through. The dimensions of these narrow corridors would not allow the scanner to be placed on a tripod; therefore, to scan these parts, a steel platform was constructed on which the scanner was mounted (Figure 4.3 (A)). TLS in this part of the cave could only be carried out during periods of very low water level in the Styx river. A total of approximately 6,000 m of these very narrow corridors were surveyed by TLS. The resulting data set from this second TLS campaign contains over 25 billion points. The next phase was cleaning and filtering the data, and this represented approximately 10% of the initial point cloud (Hofierka et al., 2017).

The key procedure in TLS data post-processing is registration where at least four common points between overlapping scans need to be co-located. This task was performed in vendor-specific software—FARO Scene™ and RIEGL RiScanPro.™

White registration spheres (Figure 4.3 (C)) were used to achieve this in the first Domica TLS survey of 2014 (Gallay et al., 2015). The scans acquired in the following campaigns by RIEGL VZ-1000 (Figure 4.3 (B)) were co-registered without any artificial targets by, first, manually finding four identical points in the overlapping scans followed by an automatic orientation. Then, an automatic multi-station adjustment (MSA) procedure was used with a robust fitting mode to closely match the scans based on their area of overlap. This step resulted in finding groups of points (i.e. polydata), which represent identical parts of the scanned surface within the specified radii. By this means, the number of points used in the subsequent MSA procedure (registration) increased, providing a more accurate registration (Ullrich et al., 2003). For the coarse registration, the standard deviation ranged from 8 to 15 mm, but after subsequent iterations of MSA, the resulting standard deviation of the internal registration of positions improved to 3 mm.

The integration of the first point cloud from 2014 with the subsequent point clouds was solved by importing all individual positions scanned in 2014 into the registration project in RiSCAN Pro and registering them with the rest of the scanned data. After the first stage of registration, the MSA procedure was used to closely match the scans which formed a closed traverse loop. The first position remained fixed with all other scan locations subsequently aligned to this initial scan. When closing the scan survey loop of the 2014 data, the accumulated standard error was markedly reduced from 150 mm to 4 mm overall. The survey traverse could not be closed in the long passage from the second water dam (east of Majkov Dome) to the Hungarian border.

To generate a continuing traverse from the underground state border with Hungary to the Majkov Dome, two water dams in the show cave part had to be crossed. This was possible due to the low water level at the time of scanning. Despite these favourable conditions, the sediment was unstable for placing the scanner securely on a tripod; therefore, a wooden platform was used in these areas (Figure 4.3 (D)). This platform was also used to move the scanner by boat between some locations saving

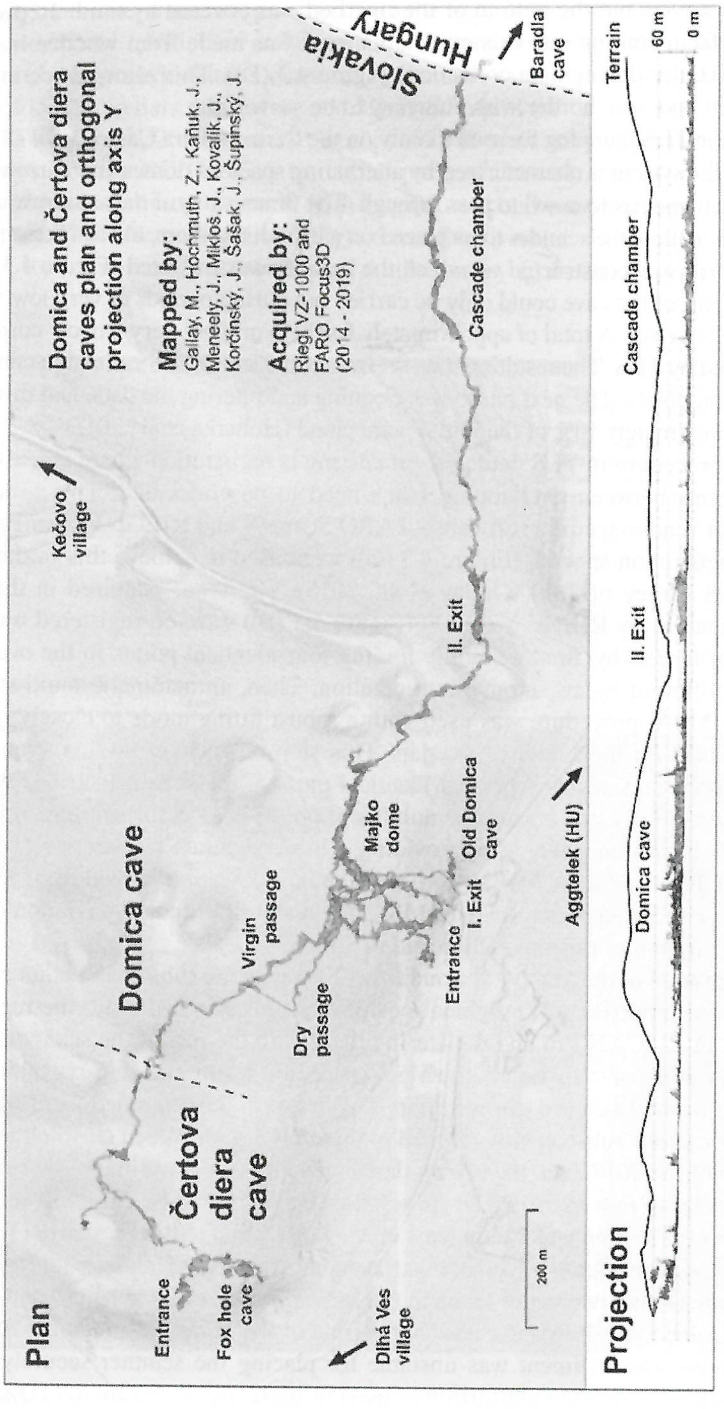

FIGURE 4.4 Top view and side view of the Domica Cave system resulting from multiple TLS campaigns combined with an airborne LiDAR digital terrain model.

valuable time in dismantling and reassembly. After scanning via the second water dam (2. plavba), the survey continued aboveground through a man-made exit from the system where control points, surveyed with an RTK-GNSS, were measured with the scanner. The registration error is at its highest in the part from the second entrance to the Hungarian border as the scanning survey traverse remains open, and the cumulated standard deviation of error was up to 200 mm. The use of artificial targets was not feasible in such extreme environmental conditions in this part of the cave; therefore, a manual selection of common points and the iterative MSA procedure was preferred as the most appropriate solution.

Redundant data, such as points from scattered reflections on sharp edges on railings, speleothems, and wet surfaces, were removed from the data set. Some mirrored features were observed when speleothems were covered with a thin film of water. Also, when scanning in winter near the cave exit, cold air mixed with the warmer air in the cave, producing a lot of noisy data on the floor and the cave ceiling. Therefore, in such environmental conditions, it is recommended to scan only when the air temperature gradient is low, ideally in light winds. After the point cloud was cleaned, its point density was unified by decimating the point cloud to a 10 mm resolution resulting in 2,000 million points. The extent of the final point cloud is shown in Figure 4.4.

Once registration was complete, the resulting point cloud was georeferenced to the national coordinate system (EPSG code: 5514 S-JTSK Křovák East North). This procedure made use of 56 points identified in the scans that were mapped by Novoveský (1975). The resulting standard deviation of transforming the data to the national coordinate system is 0.016 m. The belowground TLS cave data was supplemented with an airborne LiDAR (ALS) point cloud supplied by the company Photomap. More details on this ALS survey can be found in Hofierka et al. (2017, 2018).

Generating the 3D Cave Surface Model

The point cloud of the cave allows for precise measurements and the generation of cross-sections, plans, and visualizations. However, volume calculations and advanced analyses of the cave surface including geomorphometry or water flow modelling require the creation of a 3D digital surface model.

The key prerequisite for this task is in the calculation of normal vectors for each point to define the interior of the cave. Various approaches exist to achieve this. but for the complex cave surface morphology, the orientation of the normal is usually incorrectly determined if the normal point vectors are based on simple neighbourhood analysis. This is especially true on speleothems and various isolated geomorphological features. For this reason, normal vectors need to be oriented with respect to their scan location. After this step, the normals are correctly defined and a correct surface model of the entire cave is derived.

The 3D digital surface models (Figure 4.5) were created in the open-source software CloudCompare (Girardeau-Montaut, 2018) using the Screened Poisson surface reconstruction interpolation method (Kazhdan and Hoppe, 2013). The quality of the resulting surface depends on the presence of data voids, noise, the level of detail of the collected data, and the spatial resolution of the output model. After creating the surface model of the cave, it is necessary to extract areas of interest required for simulations.

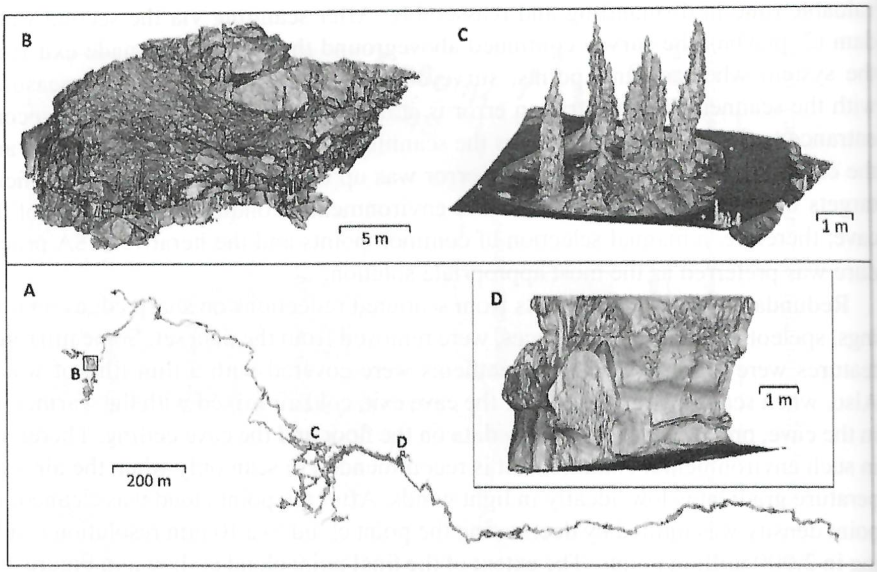

FIGURE 4.5 (A) selected parts of the 3D cave surface model, (B) showing the level of detail preserved in the model of thin ceiling stalactites, (C) massive stalagmites in the Dome of the Indian Pagodas and (D) a stegamite.

New Means of Cave Visualisation and Application

The high level of detail and spatial extent of the TLS surveyed cave system opens new possibilities for visualising and communicating its complex geometry to researchers or the general public. Traditional speleocartography can be enhanced by including planar views from the 3D model and shading/colouring the surface with a range of attributes (e.g., rock material or a morphometric parameter) (see Figure 4.6). However, a map is still a static 2D visualisation of a 3D space, and recent developments in web-based 3D technologies have enabled interactive visualisation and analysis of large 3D point clouds. It is now possible to integrate the 3D content on the Internet directly into the browser without plug-ins or additional components. For example, Silvestre et al. (2015) presented an approach in which X3-D, WebGL, and X3-DOM were used to enable online 3D visualization and navigation of the interior of the Algar do Penico Cave, Portugal, in several different Web browsers. Potenziani et al. (2015) introduced their 3-D Heritage On-line Presenter (3-DHOP), which is an open-source software package for the creation of interactive Web presentations of high-resolution 3D models. This, in turn, enhances communication of the scientific results to a wider audience, providing improved presentation, dissemination, and further analysis (Scopigno et al., 2017).

For these reasons, a stand-alone LiDAR Web portal of the cave survey was produced. This portal was generated using the Laspublish software utility in the LAStools package (Rapidlasso, 2019). This uses the Potree open-source WebGL-based renderer (Scheiblauer, 2014; Schütz, 2016; Potree, 2021). Potree is capable of efficiently

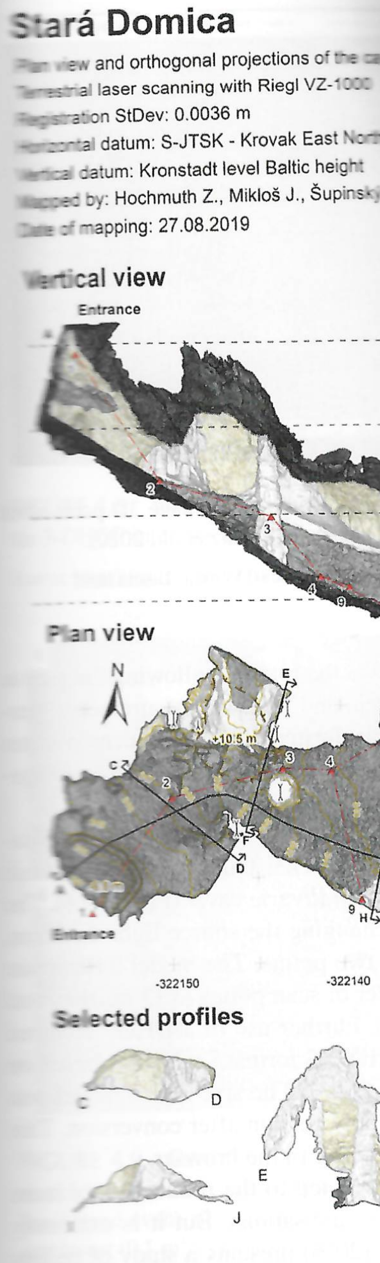

FIGURE 4.6 Example of a cave ma
Domica, Figure 4.4) resulting fro
of the cave base with the DEM colour

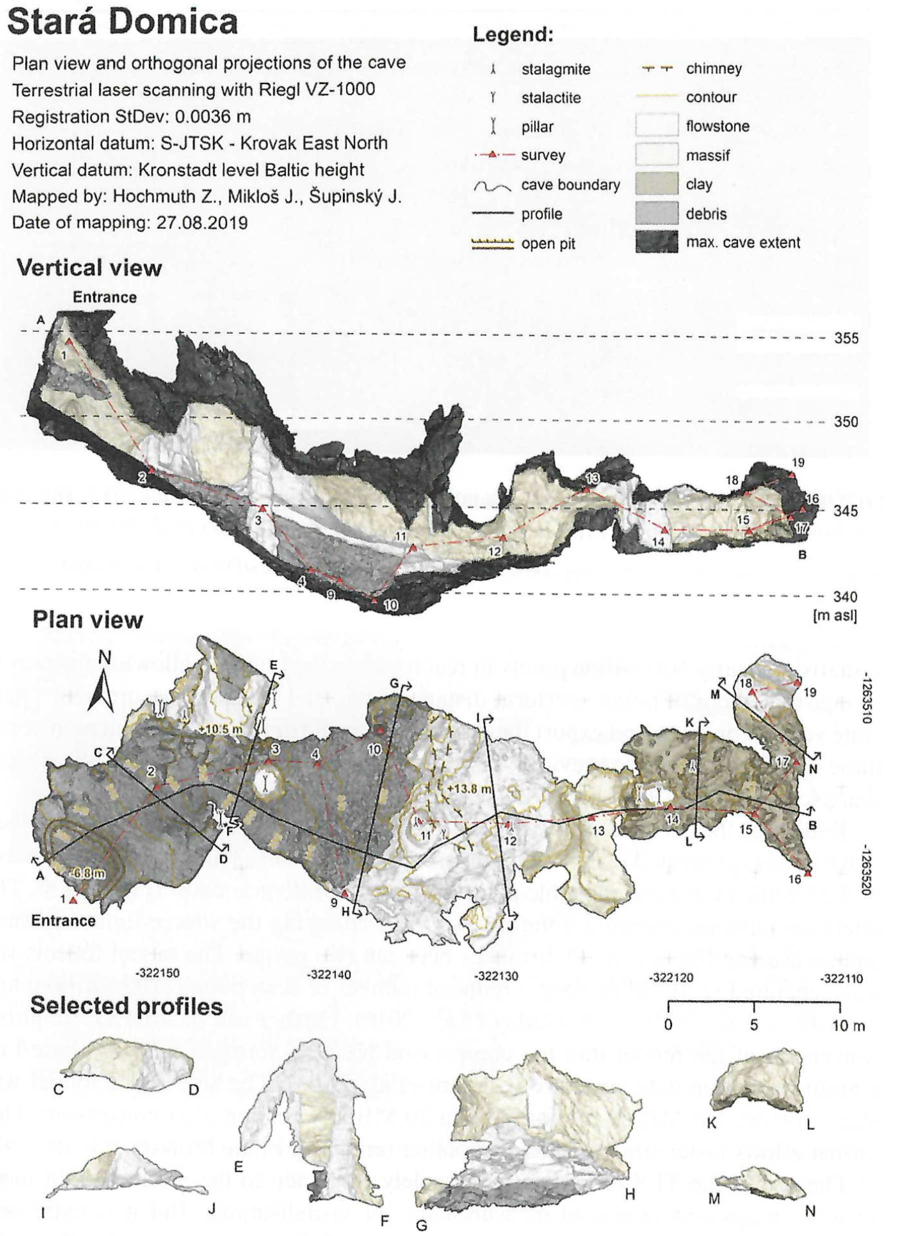

FIGURE 4.6 Example of a cave map of a part of the Domica system called Stará Domica (Old Domica, Figure 4.4) resulting from the TLS campaigns. The map contains shaded relief of the cave base with the DEM coloured according to its material.

FIGURE 4.7 Interactive online 3D visualisation and analysis of the cave 3D point cloud combined with the airborne LiDAR using the Potree interface (Schütz et al., 2020).

Source: https://uge-share.science.upjs.sk/webshared/Laspublish/Domica/Domica_Liscia.html

visualising nearly 600 billion points in real time via the Internet, allowing the user to change the colour of points; perform distance, area, and volume measurements; generate vertical profiles; and export the data in various formats. Figure 4.7 demonstrates these capabilities and the previous data set can be accessed via the link: https://uge-share.science.upjs.sk/webshared/Laspublish/Domica/Domica_Liscia.html

To display the 3D cave surface and its parameters online, an interactive visualisation tool was generated using the platform of the 3-DHOP.[1] This tool and a 3D mesh of the Domica Cave are available at http://vcg.isti.cnr.it/varie/cave/ (Figure 4.8). The interface supports zooming, rotating, panning, changing the source light direction, and measuring Euclidean 3D distances between two points. The model for this site was generated in Meshlab using a reduced number of scan points (3.13 million) and with the octree depth of 13 (Gallay et al., 2016). Further use in 3-DHOP required conversion of the model into the compressed NEXUS format,[2] which is based on a multi-resolution data structure (Cignoni et al., 2005). The size of the model was reduced from 148 MB in .ply format to a 20 MB .ply version after conversion. This format allows faster streaming and smoother rendering in the browser.

The use of the TLS cave data is not solely restricted to the production of more accurate maps and improved measurements or visualisations. But it is extremely useful in other areas of speleology. Gallay et al. (2016) presents a study of ceiling channels in the Domica system by calculating 3D morphometric parameters derived from their 3D mesh. These speleoforms are extremely inaccessible at a height of 3 m to 10 m above the base of the cave. 3D modelling of these features revealed channels and provided evidence for anastomosis (a connection between tubular structures) of the Styx river as a significant process in the formation of the cave system.

Figure 4.9 is an example of simulating a real flood event in the cave system using the Delft3D FM (D-FlowFM)[3] modelling tool in which a highly detailed 3D model of the cave floor is the main input.

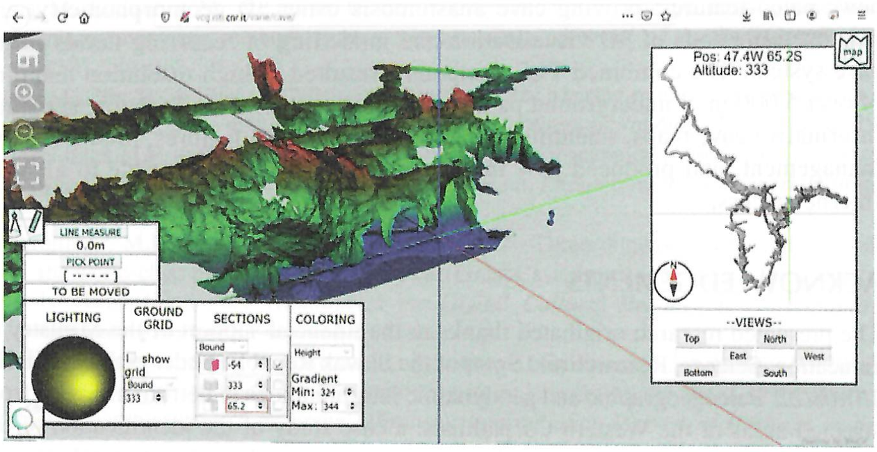

FIGURE 4.8 Interactive online 3D visualisation and analysis of the cave surface model via the 3-DHOP interface (Potenziani et al., 2015).

Source: http://vcg.isti.cnr.it/varie/cave/

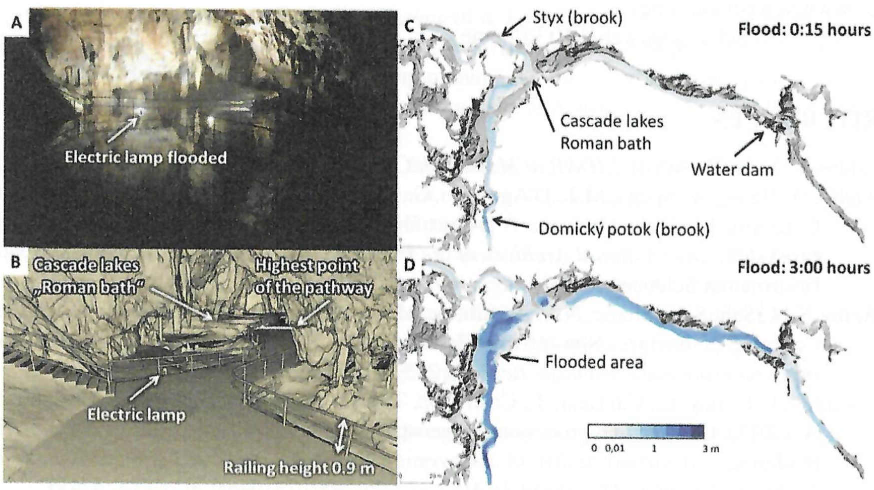

FIGURE 4.9 Cave flood modelling in the Majkov Dome (10 February 2016) with (A) a marked light source and (B) the point cloud of the dome. (C) Water depth during the simulated flood event after 15 minutes and (D) 3 hours of water inflow from the southwest and northwest (0.1 $m^3.s^{-1}$), outflow at water dam set to 0.14 $m^3.s^{-1}$.

CONCLUSIONS

The TLS survey of the Domica Cave system commenced in 2014 with a research project focused on developing new methods of 3D spatial modelling and surface analysis. The aim was to generate a 3D point cloud of the cave with ultra-high spatial resolution so that its surface morphology could be studied and possibly linked to aboveground geomorphology. This project resulted in the discovery of new speleo-features, proving cave anastomosis using 3D geomorphometry, and improved methods of 3D visualisation and modelling of recurring floods in the cave system. The combined TLS campaigns resulted in high-resolution mapping of over 5,000 m of underground passages. This data contributed to more accurate, informative cave maps, scientific research of inaccessible features, improved cave management, and produced new interactive visualisations accessible to all with Internet access.

ACKNOWLEDGEMENTS

The presented research originated thanks to the financial support of the Ministry of Education, Science, Research and Sport of the Slovak Republic under grant nr. VEGA 1/0168/22 'Paleogeographic and geodynamic interpretations of detrital minerals from selected areas of the Western Carpathians: a case study of the identification of the nature of transport conditions and source areas in karst and non-karst areas'.

NOTES

1. http://3-Dhop.net/
2. www.vcg.isti.cnr.it/nexus/
3. https://oss.deltares.nl/web/delft3d/home

REFERENCES

Addison, A. (2011, April). *LIDAR at Mammoth Cave*. Civil Engineering Surveyor, 22–25.

Aiello, D., Basso, A., Spena, M.T., D'Agostino, G., Montedoro, U., Galizia, M., . . . & Santagati, C. (2019). The virtual batcave: A project for the safeguard of a UNESCO WHL fragile ecosystem. *International Archives of the Photogrammetry*, Remote Sensing & Spatial Information Sciences.

Azmy, S.N., Sah, S.A., Shafie, N.J., Ariffin, A., Majid, Z., Ismail, N.A., & Shamsir, S. (2012). Counting in the dark: Non-intrusive laser scanning for population counting and identifying roosting bats. *Scientific Reports*, 2, 524. http://doi.org/10.1038/srep00524

Basantes, J., Godoy, L., Carvajal, T., Castro, R., Toulkeridis, T., Fuertes, W., . . . & Addison, A. (2017). Capture and processing of geospatial data with laser scanner system for 3D modeling and virtual reality of Amazonian Caves. In: *2017 IEEE Second Ecuador Technical Chapters Meeting (ETCM)*. http://doi.org/10.1109/etcm.2017.8247455

Bella, P., Littva, J., Pukanská, K., Gašinec, J., & Bartoš, K. (2015). Use of terrestrial laser scanning for the investigation of structural geological discontinuities and morphology of caves: On the example of the Dúpnica Cave, Západné Tatry Mts., Slovakia. *Acta Geologica Slovaca*, 7(2), 92–102.

Beraldin, J.A., Blais, F., Cournoyer, L., Picard, M., Gamache, D., Valzano, V., . . . & Gorgoglione, M. (2006). Multi-resolution digital 3D imaging system applied to the recording of grotto sites: the case of the Grotta dei Cervi. In: *VAST06: The 7th International Symposium on Virtual Reality, Archaeology and Intelligent Cultural Heritage*. The Eurographics Association.

Berenguer Sempere, F., Gómez-Lende, M., Serrano, E., & de Sanjosé-Blasco, J.J. (2014). Orthothermographies and 3D models as potential tools in ice cave studies: The Peña Castil Ice Cave (Picos de Europa, Northern Spain). *International Journal of Speleology*, 43(1), 35–43. http://doi.org/10.5038/1827-806X.43.1.4

Beres, M., Luetscher, M., & Olivier, R. (2001). Integration of ground-penetrating radar and microgravimetric methods to map shallow caves. *Journal of Applied Geophysics*, 46(4), 249–262.

Bosse, M., Zlot, R., & Flick, P. (2012). Zebedee: Design of a spring-mounted 3-d range sensor with application to mobile mapping. *IEEE Transactions on Robotics*, 28(5), 1104–1119.

Buchroithner, M.F., & Gaisecker, T. (2009). Terrestrial laser scanning for the visualization of a complex dome in an extreme alpine cave system. *Photogrammetrie-Fernerkundung-Geoinformation (PFG)*, 4, 329–339.

Buchroithner, M.F., Petters, C., & Pradhan, B. (2012). Three-dimensional visualization of the world-class prehistoric site of the Niah Great Cave, Borneo, Malaysia. In: Kremers, H. (Ed.), *Conference Handout at the Digital Cultural Heritage Interdisciplinary Conference*. Saint-Dié-des-Vosges, France, 2 p.

Burens, A., Grussenmeyer, P., Carozza, L., Leveque, F., Guillemin, S., & Mathe, V. (2014). Benefits of an accurate 3D documentation in understanding the status of the Bronze Age heritage cave "Les Fraux" (France). *International Journal of Heritage in the Digital Era*, 3(1), 179–196. http://doi.org/10.1260/2047-4970.3.1.179

Canevese, E.P., Forti, P., Naseddu, A., Ottelli, L., & Tedeschi, R. (2011). Laser scanning technology for the hypogean survey: The case of Santa Barbara karst system (Sardinia, Italy). *Acta Carsologica*, 40(1), 65–77.

Canevese, E.P., Tedeschi, R., Forti, P., & Mora, P. (2008). The use of laser scanning techniques in extreme contexts: The case of Naica Caves (Chihuahua, Mexico). *Geologia Tecnica & Ambientale (Journal of Technical & Environmental Geology)*, 2, 19–37.

Caprioli, M., Minchilli, M., Scognamiglio, A., & Strisciuglio, G. (2003). Using photogrammetry and laser scanning in surveying monumental heritage: le Grotte di Castellana. *International Archives of Photogrammetry Remote Sensing and Spatial Information Sciences*, 34(5/W12), 107–110.

Chamberlain, A.T., Sellers, W., Proctor, C., & Coard, R. (2000). Cave detection in limestone using ground penetrating radar. *Journal of Archaeological Science*, 27(10), 957–964.

Cignoni, P., Ganovelli, F., Gobbetti, E., Marton, F., Ponchio, F., & Scopigno, R. (2005). Batched multi triangulation. In: *IEEE Visualization, 2005, VIS 05*, 23–28 October 2005, Minneapolis, MN, 207–214. http://doi.org/10.1109/VISUAL.2005.1532797

Citton, P., Romano, M., Salvador, I., & Avanzini, M. (2017). Reviewing the upper Pleistocene human footprints from the 'Sala dei Misteri'in the Grotta della Bàsura (Toirano, northern Italy) cave: An integrated morphometric and morpho-classificatory approach. *Quaternary Science Reviews*, 169, 50–64.

Cosso, T., Ferrando, I., & Orlando, A. (2014). Surveying and mapping a cave using 3D laser scanner: The open challenge with free and open source software. *The International Archives of Photogrammetry, Remote Sensing and Spatial Information Sciences*, 40(5), 181.

Doering, T., Collins, L., & Branas, C. (2006). *Preacher's Cave High Definition Survey and 3D Laser Scanning Project*, Eleuthera, Bahamas: Scanning.

Donelan, J. (2002). Making prehistory. *Computer Graphics World*, March, pp. 32–33. Penn Well Publishing Co.

Droppa, A. (1964). Domica, plán 1:1000. *Mapový archív SMOPaJ*, ev. č. 16212.

Droppa, A. (1972). Príspevok k vývoju jaskyne Domica. *Československý kras*, 22, 65–72.

El-Hakim, S.F., Fryer, J., & Picard, M. (2004). Modelling and visualization of aboriginal rock art in the Baiame cave. *International Archives of Photogrammetry and Remote Sensing*, 35(5), 990–995.

Fabbri, S., Sauro, F., Santagata, T., Rossi, G., & De Waele, J. (2017). High-resolution 3-D mapping using terrestrial laser scanning as a tool for geomorphological and speleogenetical studies in caves: An example from the Lessini mountains (North Italy). *Geomorphology*, 280, 16–29.

Fryer, J.G., Chandler, J.H., & El-Hakim, S.F. (2005). Recording and modelling an abor inal cave painting: With or without laser scanning? *International Archives Photogrammetry, Remote Sensing and Spatial Information Sciences*, 36(5/W17), 1–

Gaál, Ľ., & Gruber, P. (2014). *Jaskynný systém Domica-Baradla*. Jaskyňa, ktorá nás sp Aggtelek (Aggteleki Nemzeti park), 512.

Gallay, M., Hochmuth, Z., Kaňuk, J., & Hofierka, J. (2016). Geomorphometric analysis cave ceiling channels mapped with 3D terrestrial laser scanning. *Hydrology and E System Sciences*, 20, 1827–1849.

Gallay, M., Kaňuk, J., Hochmuth, Z., Meneely, J., Hofierka, J., & Sedlák, V. (2015). Lar scale and high-resolution 3-D cave mapping by terrestrial laser scanning: A case st of the Domica Cave, Slovakia. *International Journal of Speleology*, 44(3), 277–29

Gašinec, J., Gašincová, S., Černota, P., & Staňková, H. (2012). Zastosowanie naziemn skaningu laserowego do monitorowania lodu gruntowego w Dobszyńskiej Jas Lodowej. *Inżynieria Mineralna*, 13, 31–42.

Gede, M., Petters, C., Nagy, G., Nagy, A., Mészáros, J., Kovács, B., & Egri, C. (20 Laser scanning survey in the Pálvölgy Cave, Budapest. In: *Proceedings of the International Cartographic Conference*. International Cartographic Associa Dresden, 905.

Girardeau-Montaut, D. (2018). *CloudCompare 2.10.2 Zephyrus*. www.cloudcompare.org

Gómez-Lende, M., & Sánchez-Fernández, M. (2018). Cryomorphological topo-graphie the study of ice caves. *Geosciences*, 8(8), 274.

González-Aguilera, D., Muñoz, A.L., Lahoz, J.G., Herrero, J.S., Corchón, M.S., & Gar E. (2009). Recording and modeling Paleolithic caves through laser scanning. In: *International Conference on Advanced Geographic Information Systems & Services*, 19–26. IEEE.

González-Aguilera, D., Muñoz-Nieto, A., Gómez-Lahoz, J., Herrero-Pascual, J., & Gutier Alonso, G. (2009). 3D digital surveying and modelling of cave geometry: Applica to paleolithic rock art. *Sensors*, 9(2), 1108–1127.

Grussenmeyer, P., Landes, T., Alby, E., & Carozza, L. (2010). High resolution 3D recording modelling of the Bronze Age cave "Les Fraux" in Périgord (France). *The Internati Archives of the Photogrammetry, Remote Sensing and Spatial Information Scien* 38, 262–267.

Hämmerle, M., Höfle, B., Fuchs, J., Schröder-Ritzrau, A., Vollweiler, N., & Frank, N. (20 Comparison of kinect and terrestrial lidar capturing natural karst cave 3-d obje *IEEE Geoscience and Remote Sensing Letters*, 11(11), 1896–1900.

Hochmuth, Z. (2014). Mapovanie prepojenia Čertovej diery a Domice. *Spravodaj Sloven speleologickej spoločnosti*, 45(3), 18–23.

Hofierka, J., Gallay, M., Bandura, P., & Šašak, J. (2018). Identification of karst sinkhole a forested karst landscape using airborne laser scanning data and water flow anal *Geomorphology*, 308, 265–277.

Hofierka, J., Šašak, J., Šupinský, J., Gallay, M., Kaňuk, J., & Sedlák, V. (2017). 3D mapov krajiny pomocou pozemného a leteckého laserového skenovania. *Životné prostre* 51, 21–27.

Kaňuk, J., Zubal, S., Šupinský, J., Šašak, J., Bombara, M., Sedlák, V., Gallay, M., Hofie J., & Onačillová, K. (2019). Testing of V3.sun module prototype for solar radia modelling on 3D objects with complex geometric structure. *International Arch of the Photogrammetry, Remote Sensing and Spatial Information Sciences—IS Archives*, 42(4/W15), 35–40.

Kaul, L., Zlot, R., & Bosse, M. (2016). Continuous-time three-dimensional mapping micro aerial vehicles with a passively actuated rotating laser scanner. *Journal of F Robotics*, 33(1), 103–132.

Kazhdan, M., & Hoppe, H. (2013). Screened poisson surface reconstruction. *ACM Transactions on Graphics (ToG)*, 32(3), 29.

Kordić, B., Đapo, A., & Pribičević, B. (2012, May). Application of terrestrial laser scanning in the preservation of fortified caves. In: *FIG Working Week 2012: Knowing to Manage the Territory, Protect the Environment, Evaluate the Cultural Heritage.* https://www.researchgate.net/publication/265025785_Application_of_Terrestrial_Laser_Scanning_in_the_Preservation_of_Fortified_Caves

Kregar, K., Vrabec, M., & Grigillo, D. (2019, January). Developing a robust workflow for acquisition of high-resolution full-3D cave topography, surface topography integration, and digital structural mapping. In: *Geophysical Research Abstracts* (Vol. 21). Copernicus Publications.

Kuda, F., Kajzar, V., Divíšek, J., & Kukutsch, R. (2014). *Aplikace pozemního laserového skenování v geovědních disciplínách.* Praha (Ústav geoniky Akademie věd České republiky, v.v.i.).

Leonov, A.V., Anikushkin, M.N., Bobkov, A.E., Rys, I.V., Kozlikin, M.B., Shunkov, M.V., . . . & Baturin, Y.M. (2014). Development of a virtual 3D model of Denisova Cave in the Altai Mountains. *Archaeology, Ethnology and Anthropology of Eurasia*, 42(3), 14–20.

Lerma, J.L., Navarro, S., Cabrelles, M., & Villaverde, V. (2010). Terrestrial laser scanning and close range photogrammetry for 3D archaeological documentation: The Upper Palaeolithic Cave of Parpalló as a case study. *Journal of Archaeological Science*, 37(3), 499–507.

Lyons-Baral, J. (2012). Using terrestrial LiDAR to map and evaluate hazards of Coronado Cave, Coronado National Memorial, Cochise County, AZ. *Arizona Geology Magazine*, Summer, 1–4.

Marsico, A., Infante, M., Iurilli, V., & Capolongo, D. (2015). Terrestrial laser scanning for 3D cave reconstruction: Support for geomorphological analyses and geoheritage enjoyment and use. In *Hydrogeological and Environmental Investigations in Karst Systems.* Springer, 543–550.

McFarlane, D.A., Buchroithner, M., Lundberg, J., Petters, C., Roberts, W., & Van Rentergem G. (2013). Integrated three-dimensional laser scanning and autonomous drone surface-photogrammetry at Gomantong caves, Sabah, Malaysia. In: Bosak, P., & Filippi, M. (Eds.), *Proceedings of the 16th International Congress of Speleology.* Brno, 2, 317–319. *Volume 2 International Congress of Speleology ICS Proceedings.* KIP Talks and Conferences. 13. https://digitalcommons.usf.edu/kip_talks/13

Milius, J., & Petters, C. (2012). Eisriesenwelt—from laser scanning to photo—realistic 3D model of the biggest ice cave on Earth. In: Jekel, T., Car, A., Strobl, J., & Griesebner, G. (Eds.), *GI-Forum 2012: Geovisualization, Society and Learning.* WichmannVerlag, Heidelberg: Salzburg, Austria, 513–523.

Mohammed Oludare, I., & Pradhan, B. (2016). A decade of modern cave surveying with terrestrial laser scanning: A review of sensors, method and application development. *International Journal of Speleology*, 45, 71–88.

Murphy, P.J., Parr, A., Strange, K., Hunter, G., Allshorn, S., Halliwell, R.A., . . . & Westerman, A.R. (2005). Investigating the nature and origins of Gaping Gill Main Chamber, North Yorkshire, UK, using ground penetrating radar and lidar. *Cave and Karst Science*, 32(1), 25.

Nash, G.H., & Beardlsey, A. (2013). The survey of Cathole Cave, Gower Peninsula, South Wales. *Proceedings of the University of Bristol Spelaeological Society*, 26(1), 73–83.

Nocerino, E., Menna, F., Farella, E., & Remondino, F. (2019). 3D virtualization of an underground semi-submerged cave system. *International Archives of the Photogrammetry, Remote Sensing and Spatial Information Sciences* (2/W15), 857–864.

Novoveský, A. (1975). *Technická správa, Domica 111-I-13.* Geologický prieskum, n.p., Geologická služba podniku, geologická oblasť Rožňava. Slovenské múzeum ochrany prírody a jaskyniarstva.

Núñez, M.A., Buill, F., & Edo, M. (2013). 3D model of the Can Sadurní cave. *Journal* *Archaeological Science*, 40(12), 4420–4428.

Perperidoy, D.G., Tzortzioti, E., & Sigizis, K. (2010). A new methodology for surveying and exp ing complex environments using 3D scanning. In: *FIG Congress*, 1–14. https://fig.net/fig20

Peterson, T., & Berg, J. (2001). *Karst mapping with geophysics at Mystery Cave S* *Park, Minnesota.* Minnesota Department of Natural Resources Ground Water Climatology Section Report, 10.

Petrović, A.S., Ćalić, J., Spalević, A., & Pantić, M. (2018). Relations between surface underground karst forms inferred from terrestrial laser scanning. *Geological Soci* *London, Special Publications*, 466(1), 107–120.

Petters, C., Milius, J., & Buchroithner, M.F. (2011). Eisriesenwelt: Terrestrial laser scann and 3D visualisation of the largest ice cave on Earth. In: *Proceedings of the Europ* *LiDAR Mapping Forum.* Salzburg, Austria, 10 p. IEEE.

Plan, L., Roncat, A., & Marx, G. (2013). Detailed morphologic analysis of palaeotraun gal using a terrestrial laser scan (Dachstein-Mammuthöhle, upper Austria). *Proceeding* *the 16th International Congress of Speleology*, 1, 399–401.

Potenziani, M., Callieri, M., Dellepiane, M., Corsini, M., Ponchio, F., & Scopigno, R. (20 3DHOP: 3D heritage online presenter. *Computers & Graphics*, 52, 129–141.

Potree. (2021). www.potree.org/ (accessed on 20 August 2021).

Pucci, B., & Marambio Castillo, A.E. (2009). Olerdola's cave, Catalonia past and pres A virtual reality reconstruction from terrestrial laser scanner and gis data. In *International Workshop 3D Virtual Reconstruction and Visualization of Comp* *Architectures*, 1–14. ISPRS.

Pukanska, K., Bartoš, K., Bella, P., & Sabová, J. (2017). Comparison of non-contact surve technologies for modelling underground morphological structures. *Acta Montanis* *Slovaca*, 22(3), 246–256.

Radicioni, F., Rossi, G., Tosi, G., & Marsili, R. (2019, May). Non contact shape and dimen measurements by LIDAR techniques of one of the biggest Italian caverns. *Journa* *Physics: Conference Series*, 1249(1), 012019. IOP Publishing.

Rapidlasso GmbH. LAStools. https://rapidlasso.com/lastools/ (accessed on 1 August 201

Robson-Brown, K., Chalmers, A., Saigol, T., Green, C., & D'errico, F. (2001). An autom laser scan survey of the Upper Palaeolithic rock shelter of Cap Blanc. *Journa* *Archaeological Science*, 28(3), 283–289.

Roncat, A., Dublyansky, Y., Spötl, C., Dorninger, P., & Pfeifer, N. (2011). A full-3D la scan mapping of a hypogene cave: A morphogenetic study of Märchenhöhle, Aus *Geophysical Research Abstracts. EGU 2011, Vienna*, 13, 14039.

Rüther, H., Chazan, M., Schroeder, R., Neeser, R., Held, C., Walker, S.J., . . . & Horwitz, L (2009). Laser scanning for conservation and research of African cultural heritage s The case study of Wonderwerk Cave, South Africa. *Journal of Archaeological Scie* 36(9), 1847–1856.

Santagata, T., Lugli, S., Camorani, M.E., & Ercolani, M. (2015). Laser scanner survey an view applications of the "Grotta della lucerna" (Ravenna, Italy), a roman mine for specularis. In *Hypogea 2015: Proceedings of International Congress of Speleolo* *Artificial Cavities: Italy*, Rome, 11/17 March 2015, 1, 411–416.

Santos Delgado, G., Martínez Rubio, J., Silva Barroso, P.G., Sánchez Moral, S., Caña Jiménez, J.C., & De la Rasilla Vives, M. (2012). Contribución al conocimiento cueva de El Sidrón (Piloña, Asturias) con técnicas de láser escáner 3D. In: Gonz A., et al. (Eds.), *Avances de la Geomorfología en España 2010–2012. Actas de la* *Reunión Nacional de Geomorfología, Santander*, 17–20 September 2012, 255– Editorial Universidad de Cantabria, Santander.

Scheiblauer, C. (2014). *Interactions with Gigantic Point Clouds*. Ph.D. Thesis, Vienna University of Technology, Vienna, Austria, 203.

Schütz, M. (2016). *Potree: Rendering Large Point Clouds in Web Browsers*. Engineer Diploma Thesis, Vienna University of Technology, Vienna, Austria, 92.

Schütz, M., Ohrhallinger, S., & Wimmer, M. (2020). Fast out-of-core octree generation for massive point clouds. *Computer Graphics Forum*, 39(7), 1–13.

Scopigno, R., Callieri, M., Delleppiane, M., Ponchio, F., & Potenziani, M. (2017). Delivering and using 3D models on the web: Are we ready? *Virtual Archaeology Review*, 8, 1–9.

Silvestre, I., Rodrigues, J.I., Figueiredo, M., & Veiga-Pires, C. (2015). High-resolution digital 3D models of Algar do Penico Chamber: Limitations, challenges, and potential. *International Journal of Speleology*, 44(1), 25–35. http://doi.org/10.5038/1827-806X.44.1.3

Stipanov, M., Bakarić, V., & Eškinja, Z. (2008). ROV use for cave mapping and modeling. *IFAC Proceedings Volumes*, 41(1), 208–211.

Šupinský, J., Kaňuk, J., Hochmuth, Z., & Gallay, M. (2019). Detecting dynamics of cave floor ice with selective cloud-to-cloud approach. *The Cryosphere*, 13(11), 2835–2851.

Thibault, G. (2001). 3D modeling of the Cosquer cave by laser survey. *International Newsletter on Rock Art, No. 28*, 25–29. https://www.bradshawfoundation.com/inora.php

Triantafyllou, A., Watlet, A., Le Mouélic, S., Camelbeeck, T., Civet, F., Kaufmann, O., . . . & Vandycke, S. (2019). 3-D digital outcrop model for analysis of brittle deformation and lithological mapping (Lorette cave, Belgium). *Journal of Structural Geology*, 120, 55–66.

Tsakiri, M., Sigizis, K., Billiris, H., & Dogouris, S. (2007, September). 3D laser scanning for the documentation of cave environments. In *11th ACUUS Conference: Underground Space: Expanding the Frontiers*. http://www.minetech.metal.ntua.gr/

Tyszkowski, S., Kramkowski, M., Wisniewska, D., & Urban, J. (2016, April). Use of terrestrial laser scanning for the documentation of quaternary caves. In *EGU General Assembly Conference Abstracts* (Vol. 18). Copernicus Publications.

Ullrich, A., Schwarz, R., & Kager, H. (2003). Using hybrid multi-station adjustment for an integrated camera laser-scanner system. https://publik.tuwien.ac.at/files/PubDat_119447.pdf

Wenger, R. (2004). La balise de positionnement U-GPS (Underground-GPS). *ISSKA Rapport Annuel* (Swiss Institute for Speleology and Karst Studies, La Chaux-de-Fonds 2004), 13–14. http://www.isska.ch/pdf/Fr/Rapport_annuel/rapp_annuel_04.pdf

Westerman, A.R., Pringle, J.K., & Hunter, G. (2003). Preliminary LIDAR survey results from Peak Cavern Vestibule, Derbyshire, UK. *Cave and Karst Science*, 30(3), 129–130.

Yakar, M., Ulvi, A., & Toprak, A.S. (2016). The use of laser scanner in caves, encountered problems and solution suggestion. *Universal Journal of Geoscience*, 4(4), 81–88.

Zeid, N.A., Bignardi, S., Russo, P., & Peresani, M. (2019). Deep in a Paleolithic archive: Integrated geophysical investigations and laser-scanner reconstruction at Fumane Cave, Italy. *Journal of Archaeological Science: Reports*, 27, 101976.

Zlot, R., & Bosse, M. (2014). Three-dimensional mobile mapping of caves. *Journal of Cave & Karst Studies*, 76(3).

7 Unpiloted Airborne Laser Scanning of a Mixed Forest

A Case Study from the Alps, Austria

Michal Gallay, Ján Kaňuk, Carlo Zgraggen, Benedikt Imbach, Ján Šašak, Jozef Šupinský, and Markus Hollaus

INTRODUCTION

Unpiloted airborne laser scanning (ULS) mounted on a multirotor or a helicopter platform combined with low-altitude flight and relatively slow speeds produce point densities that are orders of magnitude greater than traditional airborne laser scanning. The ULS of forests has also produced point clouds with densities equivalent to terrestrial LiDAR scanning (TLS), which has its drawbacks in the occlusion of tree digitization and the limited efficiency and mobility of the TLS system setup on the ground (Wang et al., 2019). ULS laser scanning coupled with wide-scan angles produces point densities that can resolve individual tree and branch structures similar to those collected by TLS (Morsdorf et al., 2017; Wieser et al., 2017; Kellner et al., 2019; Brede et al., 2019). Low-altitude flight also reduces the impact of Global Navigation Satellite Systems (GNSS) positioning uncertainties that can increase with the distance between the sensor and the terrain. Recent developments have shown that the application of ULS is possible even under the forest canopy providing accurate and ultra-detailed point clouds (Hyyppä et al., 2020). Because drone flight is predominantly under the control of the investigator and is normally one order of magnitude less costly than traditional airborne laser scanning, flight plans can be developed to collect high-density measurements in novel ways that enable hypothesis testing or to evaluate the impact of various data collection strategies on remote sensing measurements.

A summary of current lightweight laser scanners suitable for UAS and their key properties is listed in Table 7.1. The majority of these systems, including all of the RIEGL units, are mechanical—in that they rely predominantly on rotating mirrors to emit and collect the returning laser. The rest of the systems are lighter and smaller.

DOI: 10.1201/9780429327575-7

TABLE 7.1
Summary of Lightweight Laser Scanners Suitable for UAS-Based on Manufacturer Specifications

Manufacturer/Model	Weight (kg)	Range Accuracy (cm)	Beam Divergence (mrad)	Laser Wavelength (nm)	Max. Measurement Rate (kHz)	No. Returns	Max. Measurement Range (m)	Horizontal FOV (deg.)
RIEGL/VUX-120	2	1	0.4	1550	1800	Multiple	720	100
RIEGL/VUX-240	3.8	2.0	0.35×0.35	1550	1500	Multiple	350	75
RIEGL/VUX-1	3.5	1.0	0.5×0.5	1550	500	Multiple	170	330
RIEGL/VUX-1HA	5.0	0.5	0.5×0.5	1550	1000	Multiple	120	360
RIEGL/VUX-1LR	3.5	1.5	0.5×0.5	1550	750	Multiple	215	330
RIEGL/miniVUX-1	1.55	1.5	1.6×0.5	905	100	5	150	360
RIEGL/miniVUX-3	1.55	1.5	1.6×0.5	905	200	5	330	360
Velodyne/Puck LITE	0.59	3	-	905	600	2	100	360
Velodyne/HDL-32E	1.0	2.0	3.0×1.5	905	695	2	100	360
Velodyne/Velarray h800	1.0	3	-	905	400	1	200	120
Ibeo/LUX 4L	1.0	10	1.4×1.4	905	18.5	3	200	110
Hokuyo/UTM-30LX	0.37	3.0–5.0	-	905	4.3	1	270	270
Sick/LD-MRS 420201	0.77	10.1	1.4 × 1.4 × 2.8	905	-	3	300	110
Hesai/Pandar40	1.46	2	3	905	720	2	200	360
Hesai/Pandar64	1.52	2	3	905	720	2	200	360
Ouster/OS2–32	1.1	3–10	1.6	865	655	1	240	360
Ouster/OS2–128	1.1	3–10	1.6	865	2500	1	240	360
Quanergy/M8-Ultra	0.9	3	-	905	420	3	200	360
Livox/Mid-40	0.7	2	-	905	100	1	260	98

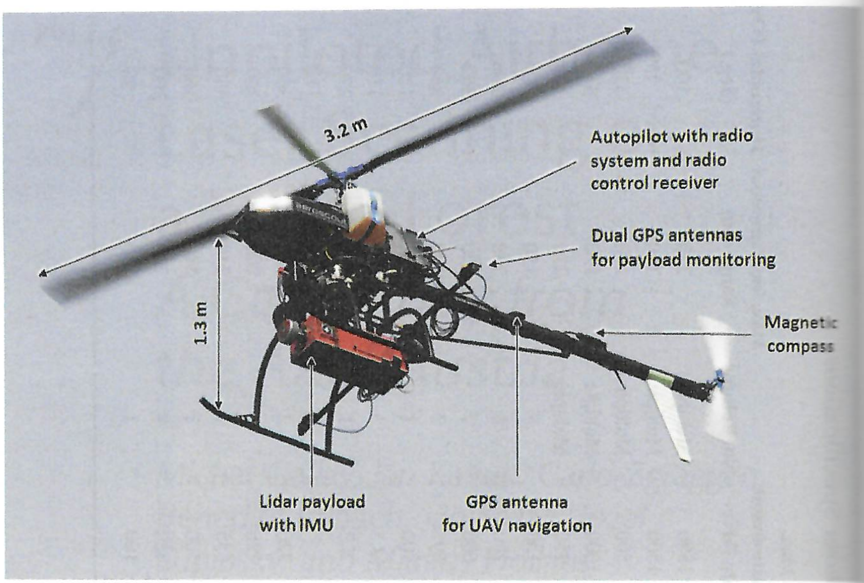

FIGURE 7.1 The unpiloted helicopter system Scout B1–100 by Aeroscout GmbH with laser scanning payload at the site near Düns, Vorarlberg, Austria.

and their primary application is in advanced driver assistance systems (ADAS) and autonomous navigation (Lambert et al., 2020). They use a rotating array of laser emitters comprising 16 to 128 laser light emitters (channels) except the Livox and Velodyne Velarray devices. The two Ouster models are unique with their mechanically rotating, multi-beam flash LiDAR, which produces structured point clouds. The most recent advances in ULS use a solid-state LiDAR with no rotating components, such as in the Livox MID-40 or Velodyne Velarray H800, and in the near future, these solid-state scanners are likely to outperform those based on mechanical rotation. The performance of five of these ULS systems listed in Table 7.1, over three different kinds of landscapes are compared in Hu et al. (2021).

This case study from the Central Eastern Alps of Vorarlberg, Austria, used an unpiloted helicopter system, Scout B1–100, that was equipped with a VUX- LiDAR system and demonstrates the use of the data acquired in assessing local geomorphology, tree segmentation, and 3D modelling of solar irradiation with ULS (Kaňuk et al., 2018) (Figure 7.1). The LiDAR system used in this research, although relatively old, was chosen because of its measurement accuracy, the number of laser returns and on-the-fly full-waveform processing. Additional results from this project can be found in Bruggisser et al. (2019).

AREA OF INTEREST

In this study, the LiDAR data acquisition covered an area between the villages of Düns and Dünserberg, Vorarlberg, Austria, with central geographic coordinates 47°13'20.83" N and 9°43'42.28" E (WGS84) (Figure 7.2). The total area mapped

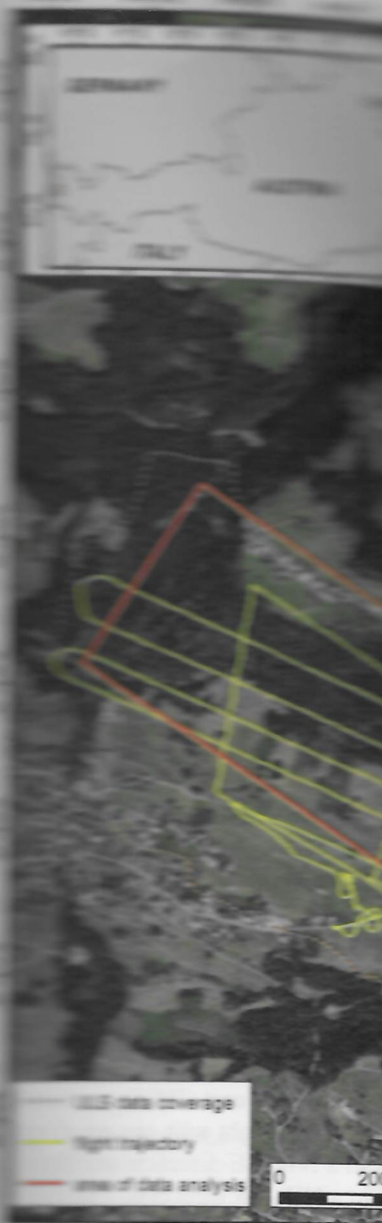

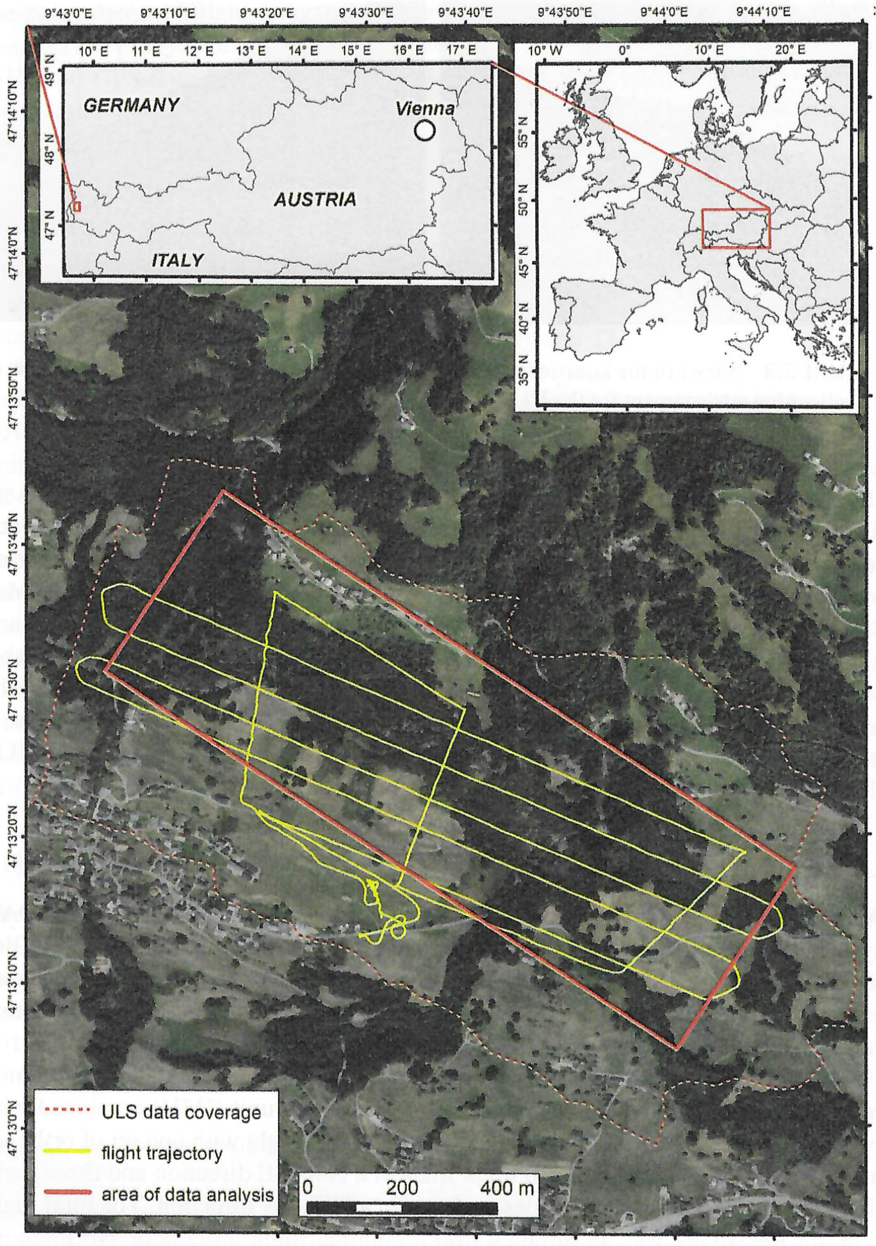

FIGURE 7.2 Location of the area of interest with flight lines, data coverage, and area of interest used in the analysis.

was 1.25 km^2, and this study focuses on the area outlined by the large red rectangle and covers 0.675 km^2 (1500 x 450 m). The area of interest is predominantly covered by mixed forest, dominated by coniferous trees (mainly spruce), and the elevation ranges from 800 to 1140 m.a.s.l. The trees grow on steep slopes (20–50°) where

FIGURE 7.3 Views of the laser-scanned steep slope near Dünserberg provide impression of a challenging environment for the ULS mission.

shallow landslides also occur (Figure 7.3). The mean canopy heights are 11.5 m. These topographic parameters made it challenging to conduct a ULS survey and required careful mission planning. Flight permission was approved by the Austrian aviation authority, Austro Control, and the survey was carried out on the 30 May 2017 just before midday. The weather was sunny, with a light breeze of 4 m.s^{-1} and air temperature of 25 °C. With such a heavy UAS, site accessibility and a suitable takeoff/landing location are important aspects of a successful survey mission. The area of interest was easily accessible by a local asphalt road so that all equipment needed for the flight could be transported by a van adjacent to the place of takeoff in the central part on a meadow.

ULS FLIGHT MISSION AND DATA PROCESSING

Aeroscout GmbH manufactured the helicopter and integrated it with the LiDAR system. The details of the technology used are summarized in Gallay et al. (2016) and Kaňuk et al. (2018). The laser scanner is a time-of-flight, pulse-based system, emitting infrared pulses of 1550 nm wavelength with a maximal pulse repetition frequency of 500 kHz.

The location, attitude, and orientation of the scanner during data collection is recorded by an Oxford xNAV550 inertial measurement unit (IMU) combined with two GPS antennas. The data was collected in a single flight with one set of orthogonal flight lines, comprising seven flight lines in a NW–SE direction and three flight lines, approximately at right angles to these, in a NE–SW direction. The total flight time for the survey was 48 minutes with a nominal flight altitude of 110 m above ground level and average flight speed of 6 m·s^{-1}. Given the scanners beam divergence of 0.5 mrad, the scan angle was limited to 90° and the scan density ranged from 4 cm between measurements at the canopy of the tallest trees to 6 cm open ground.

During the autonomous part of the flight, the flight control system maintained stable control of the aircraft and sensors. For example, during a representative flight line, the standard deviation of flight speed was 0.06 m.s^{-1}, and the accuracy in the pitch, roll, and heading axes was 0.05°, 0.06°, and 0.09°, respectively. The quality of the post-processed flight trajectory defines the absolute accuracy of the ULS point cloud. This post-processing was performed in NAVsolve software by OXTS. The IMU and GPS data from the onboard ULS payload were integrated with the GPS base station recordings, resulting in an absolute accuracy of flight trajectory of 2–8 mm in WGS84 coordinates.

SUPPLEMENTARY DATA FROM UAV CLOSE-RANGE PHOTOGRAMMETRY AND TERRESTRIAL LASER SCANNING

In addition to mapping by ULS, two other methods of high-resolution mapping were used to compare this data—drone photogrammetry and TLS.

Close-range drone-based photogrammetry was used to derive a point cloud and a colour orthoimage of the study site. Overlapping images, collected using a DJI Phantom 4 UAV, were processed in Agisoft Metashape software, producing a point cloud and an orthoimage. The average point density over this UAV mapped 0.56 km^2 area was 187 points.m^{-2}. The average ground sampling distance (GSD–average pixel size) of the orthomosaic was 4.5 cm. For comparison with ULS and UAV point clouds, a small area was also surveyed using a RIEGL VZ-1000 terrestrial LiDAR system (TLS) system. This long-range, tripod-mounted scanner was used to collect detail on the slope and trees from three locations. These three data sets were then registered (joined together) using RiScanPro software with a combined error of 8 mm. The UAV and TLS point clouds were then co-registered with respect to the ULS data using RiScanPro software and multi-station adjustment with an accuracy of 80 mm and 95 mm, respectively. No GPS ground control points were used.

CHARACTERISTICS OF THE ULS POINT CLOUD

The ULS point cloud contained 432 million unique laser returns with an average density of 345.74 points·m^{-2}, ranging from 100 up to 2000 points·m^{-2} (Figure 7.4). In comparison, the average point density of traditional, piloted, airborne LiDAR data collected by the State of Vorarlberg is circa 30 points·m^{-2} (Bruggisser et al., 2019). The mean density of first returns over the forested section of the study area was 1850 points·m^{-2} with 105 ground points·m^{-2} on average. Laser pulses

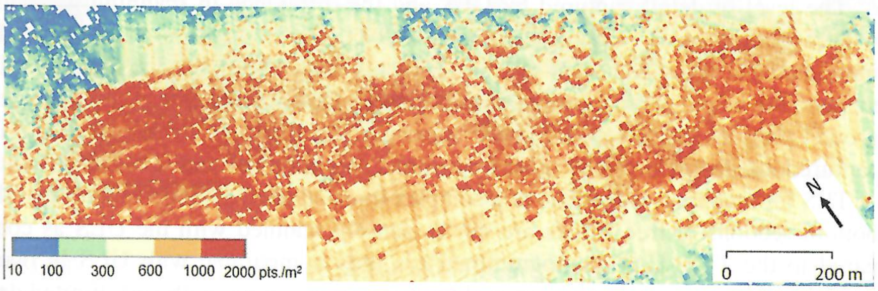

FIGURE 7.4 Point density of the ULS point cloud calculated in 5 x 5 meter cells.

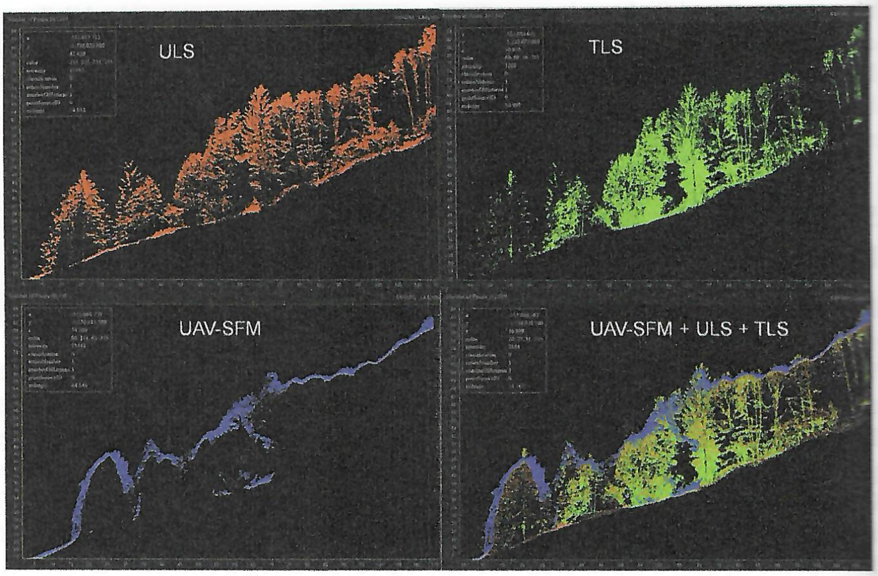

FIGURE 7.5 Vertical cross-section of a forest mapped by unpiloted airborne LiDAR (ULS), unpiloted close-range photogrammetry (UAV-SFM), and terrestrial LiDAR (TLS). The profile line is located in Figure 7.7.

emitted from the ULS reflect from objects both on and above the ground surface (e.g., vegetation, buildings, and bridges). One emitted laser pulse can return to the LiDAR sensor as one or a number of returns. Any emitted laser pulse that encounters multiple reflection surfaces as it travels in the direction of the ground is split into as many returns as there are reflective surfaces. The first returned laser pulse is the most important return and will come from the highest feature in an area like a treetop or the top of a building. However, the first return can also represent the ground, in which case only one return will be detected by the ULS. Multiple returns can be used to detect the elevation of several objects within the laser footprint of an outgoing laser pulse. These intermediate returns are generally used to determine vegetation structure, with the last return used for bare-earth (vegetation free) terrain models.

The level of detail captured by ULS and the difference in scanning geometry with respect to the UAV photogrammetry and TLS point clouds are clear from the individual and combined cross-sections in Figure 7.5. Overall, the ULS successfully mapped the whole vertical profile of the site. The benefit of TLS is clear in the near ground portions of the forest, but the upper parts of the trees are not satisfactorily captured due to occlusion by other tree trunks and branches and this limits the use of TLS for mapping wide areas of a complex forested environment. Conversely, the bottom sections of tree trunks are not as densely scanned with the ULS as compared to the TLS. UAV photogrammetry is only comparable with ULS in open non-vegetated areas and only captured the vegetation canopy with very limited data on tree structure or terrain under the forest canopy.

Vegetation cover was categorized by the use of filtered and classified returns of the ULS data. Figure 7.6 shows a cross-section and perspective view of the point cloud coloured by vegetation, ground, and buildings and illustrates the high level of detail acquired using this system. The height difference between the first and last ground return (normalized height) presented in Figure 7.7 shows the distribution of vegetation canopy height. Areas with the darkest blue indicate trees taller than 30 m.

Being able to map the terrain below any vegetation is not only vital for calculating vegetation height, but it can also be used to identify geomorphological features and clues to the processes that formed them. The ULS ground returns were used to derive a digital terrain model (DTM) of the study area. The series of maps in Figure 7.8, produced using GRASS GIS software, show some basic geomorphometric parameters derived from the DTM. The central part of the area comprises undulating terrain under the forest (Figure 7.7). This is the result of shallow landslides. Inclination of some the trees in the cross-section of Figure 7.6 also indicate historic soil movement. This DTM can also be used to model environmental phenomena directly affected by the topography such as snow thaw, solar irradiation, and species distribution.

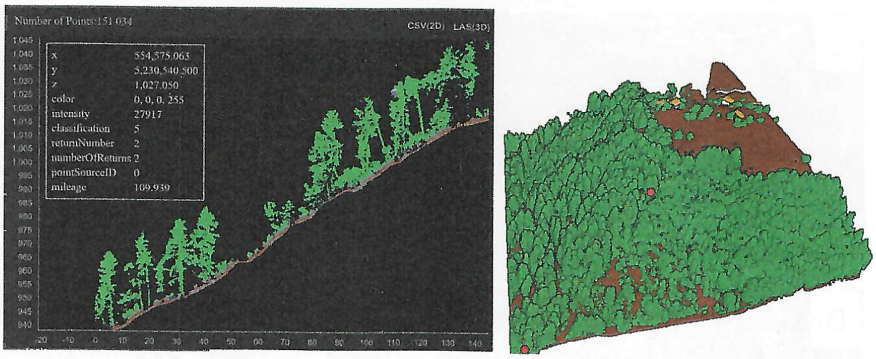

FIGURE 7.6 Cross-section and 3D perspective view of the classified UAS LiDAR point cloud. The location of cross-scetion is marked with red dots in perspective view, and this transect is also shown in Figure 7.7 (red line).

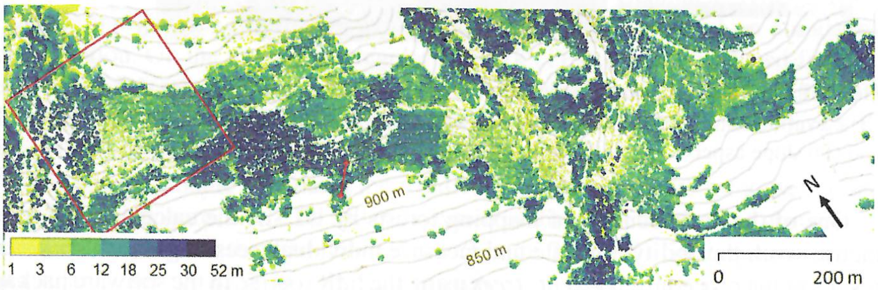

FIGURE 7.7 Vegetation canopy height model derived from points higher than 1 meter above ground level. The red line locates the cross-section in Figure 7.5 and 7.6 and the red box delineates the area in perspective view in Figure 7.6

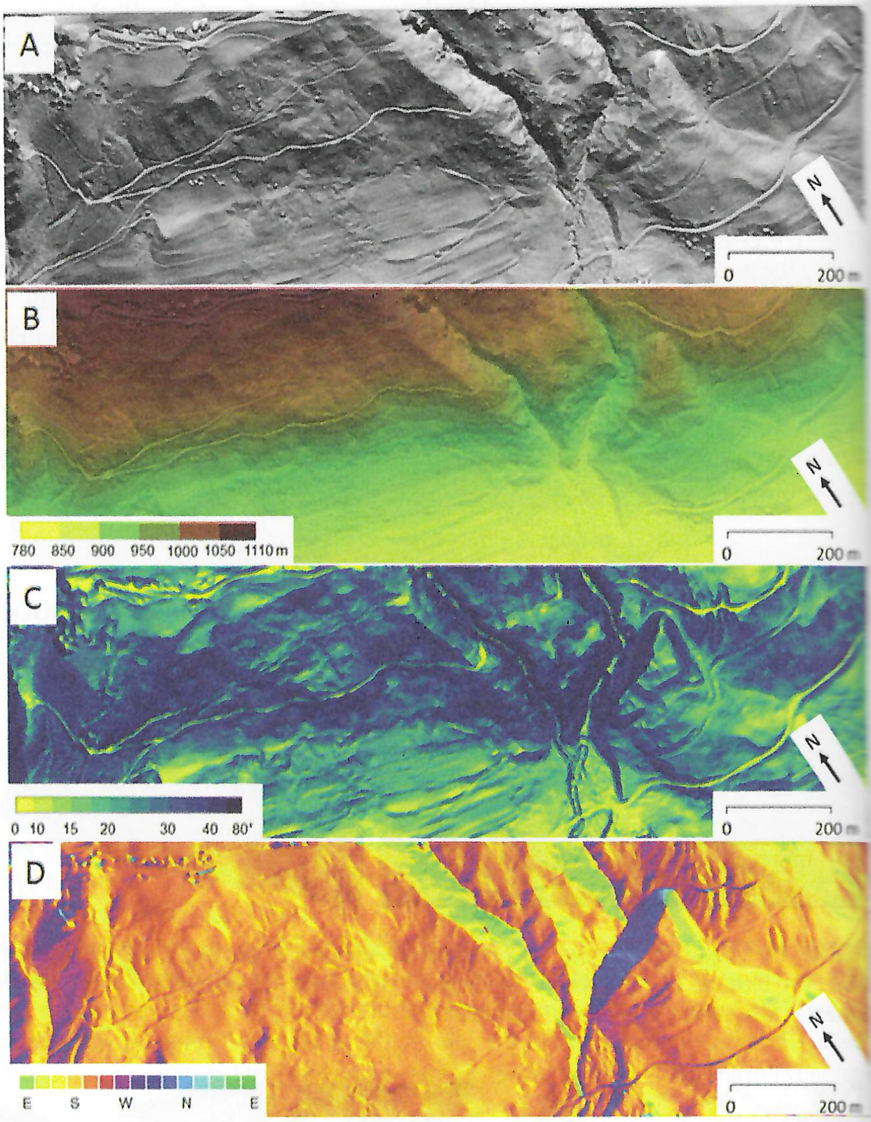

FIGURE 7.8 Digital terrain model derived as a grid of 0.2 metre cell size. (A) shaded relief (B) elevation combined with shaded relief and using a grid of 2 metre cells (C) slope angle and (D) slope aspect.

One of the main benefits of mapping forests by ULS is the calculation of forest metrics with the ability to locate and measure individual trees. Figure 7.9 shows the results of the procedure *segment_trees* using the lidR routine in the software package R (Roussel et al., 2020). Location of the area is marked by the red square in Figure 7.7. This high data density and accuracy could be used to calculate ground biomass

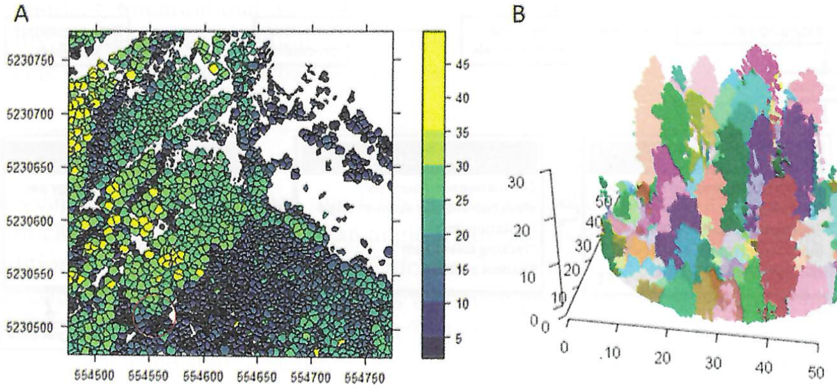

FIGURE 7.9 (A) Polygons delineating segmented trees from the ULS point cloud coloured by maximum tree height in meters. (B) A 3D perspective view of a group of segmented trees with unique tree colours from the area marked with red circle in A. The units of axes coordinates are in meters.

estimate log production volumes, and aid forest management plans (Bruggisser et al., 2020).

MODELLING SOLAR IRRADIATION ON TREES

Contemporary solar modelling tools do not allow for modelling the solar irradiation simultaneously for a ground surface and tress.

To calculate this, the program v3.sun, which is designed for modelling solar energy in high spatial resolution across areas of several square kilometers on complex 3D objects was used (Kaňuk et al., 2019). The workflow for this program is shown in Figure 7.10. This program is run via a series of steps using GRASS GIS Shell Scripts and uses data structures derived by adaptive triangulation from 3D point clouds.

3D models of the area of interest (Figure 7.11 (A)) were derived from the ULS point cloud using 3D Delaunay triangulation applied in Geomagic Wrap software (Edelsbrunner et al., 1998). This is an interpolation method based on an adaptive triangulation. On the triangular irregular network (TIN) surface produced from this modelling, it is necessary to orient the normals of the surface for each triangle to the sun (Figure 7.11 (C)). Determining this orientation of triangle normals plays a key role in preparing the input data for modelling solar irradiation.

The v3.sun module calculates the irradiance/irradiation value for a user-defined time interval (Figure 7.10 (F1)), and the position of the sun is determined according to a defined step within the astronomical day (Figure 7.10 (F2)). Subsequently a tracking solar beam for each face of each triangle is produced. The result is stored in the 'energy' parameter as $W.m^{-2}$ (watts per square meter). Thus, it is the amount of energy that has impacted on the area of the face of triangle.

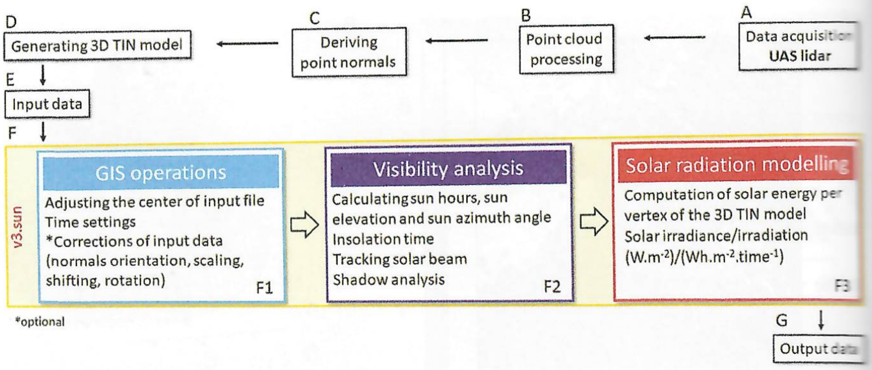

FIGURE 7.10 Workflow of solar radiation modelling on the 3D forest mesh by the v3.sun module prototype.

Source: Kaňuk et al., 2019

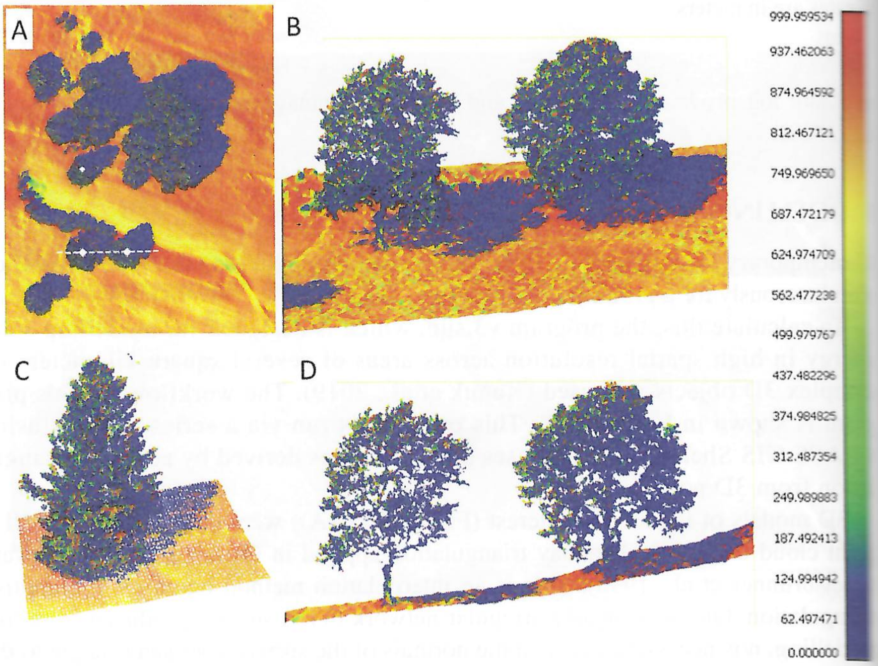

FIGURE 7.11 3D mesh from the ULS data coloured by direct solar irradiation ($W.m^{-2}$) on 21 June 2017, 12:00 local time, generated using v3.sun. Top orthogonal view (A) shows the location of the tree tops displayed in the 3D views of (B) and (C). The dashed line in (A) locates the vertical cross-section in (D).

The advantage of this approach is a highly detailed model of solar energy incident to the tree and the surface below, regardless of the geometric complexity of the tree. The 3D mesh of the 100 m x 100 m selected area and the results from this process are shown in Figure 7.11. This scene contains 6 million facets/triangles. It is the authors' intention that the v3.sun program will become an open-access tool for highly detailed solar radiation modelling for geometrically complex 3D landscape objects such as forests or urban landscapes.

CONCLUSIONS

This case study demonstrated that ULS enables the collection of ultra-high-density point clouds using wider laser scan angles than have been previously possible from traditional higher altitude airborne platforms. These low-altitude drone flights make it possible to acquire 3D measurements with high precision and accuracy, achieving point densities of thousands of points.m^{-2}. On forests, this data can be used to clearly resolve branch and stem structures, comparable to TLS and is acquired more rapidly over large landscapes at a fraction of the cost of traditional airborne laser scanning. Dense 3D point clouds, capturing the complexity of the vertical tree profiles, open opportunities to model complex natural phenomena such as solar energy. Unpiloted laser scanning is not a replacement for piloted airborne platforms or TLS. ULS represents a binding link between ALS and TLS, providing point clouds with levels of detail close to TLS, while facilitating a more time-efficient acquisition of larger areas, amounting typically to several hectares. Drone-based flight operations provide flexibility and enable access to locations where traditional flight operations are challenging, either because the sites are remote or because permissions are difficult to secure. The market of lightweight LiDAR systems and drone platforms is growing rapidly providing wide range of technological solutions. Further reduction in size and weight with an increase in device performance paves a very promising future for smaller and lighter ULS systems.

ACKNOWLEDGEMENTS

The presented research originated thanks to the financial support of the Ministry of Education, Science, Research and Sport of the Slovak Republic under the grant nr. VEGA 1/0085/23 'Modeling urban heat islands using geospatial tools'.

REFERENCES

Brede, B., Calders, K., Lau, A., Raumonen, P., Bartholomeus, H.M., Herold, M., Kooistra, L. 2019. Non-destructive tree volume estimation through quantitative structure modelling: Comparing UAV laser scanning with terrestrial lidar. *Remote Sensing of Environment* 233, Article 111355.

Bruggisser, M., Hollaus, M., Kükenbrink, D., Pfeifer, N. 2019. Comparison of forest structure metrics derived from UAV lidar and ALS data. *ISPRS Annals of the Photogrammetry, Remote Sensing and Spatial Information Sciences* 4(2/W5), 325–332.

Bruggisser, M., Hollaus, M., Otepka, J., Pfeifer, N. 2020. Influence of ULS acquisition characteristics on tree stem parameter estimation. *ISPRS Journal of Photogrammetry and Remote Sensing* 168(2020), 28–40.

Edelsbrunner, H., Facello, M.A., Fu, P., Qian, J., Nekhayev, D.V. 1998. Wrapping 3D scanning data. In *Three-Dimensional Image Capture and Applications* (Vol. 3313, pp. 148–159). International Society for Optics and Photonics.

Gallay, M., Eck, C., Zgraggen, C., Kaňuk, J., Dvorný, E. 2016. High resolution airborne laser scanning and hyperspectral imaging with a small UAV platform. *The International Archives of the Photogrammetry, Remote Sensing and Spatial Information Sciences* XLI-B1, 823–827.

Hu, T., Sun, X., Su, Y., Guan, H., Sun, Q., Kelly, M., Guo, Q. 2021. Development and performance evaluation of a very low-cost UAV-lidar system for forestry applications. *Remote Sensing* 13(1), 77.

Hyyppä, E., Hyyppä, J., Hakala, T., Kukko, A., Wulder, M.A., White, J.C., Pyörälä, J., Yu, X., Wang, Y., Virtanen, J.-P., Pohjavirta, O., Liang, X., Holopainen, M., Kaartinen, H. 2020. Under-canopy UAV laser scanning for accurate forest field measurements. *ISPRS Journal of Photogrammetry and Remote Sensing* 164, 41–60.

Kaňuk, J., Gallay, M., Eck, C., Zgraggen, C., Dvorný, E. 2018. Technical report: Unmanned helicopter solution for survey-grade lidar and hyperspectral mapping. *Pure and Applied Geophysics* 175(9), 3357–3373.

Kaňuk, J., Zubal, S., Šupinský, J., Šašak, J., Bombara, M., Sedlák, V., Gallay, M., Hofierka, J., Onačillová, K. 2019. Testing of V3.sun module prototype for solar radiation modelling on 3D objects with complex geometric structure. *International Archives of the Photogrammetry, Remote Sensing and Spatial Information Sciences—ISPRS Archives* 42(4/W15), 35–40.

Kellner, J.R., Armston, J., Birrer, M., Cushman, K.C., Duncanson, L., Eck, C., Falleger, C., Imbach, B., Král, K., Krůček, M., Trochta, J., Vrška, T., Zgraggen, C. 2019. New opportunities for forest remote sensing through ultra-high-density drone lidar. *Surveys in Geophysics* 40(4), 959–977.

Lambert, J., Carballo, A., Cano, A.M., Narksri, P., Wong, D., Takeuchi, E., Takeda, K. 2020. Performance analysis of 10 models of 3D LiDARs for automated driving. *IEEE Access* 8, Art. no. 9142208, 131699–131722.

Morsdorf, F., Eck, C., Zgraggen, C., Imbach, B., Schneider, F.D., Kükenbrink, D. 2017. UAV-based LiDAR acquisition for the derivation of high-resolution forest and ground information. *Leading Edge* 36(7), 566–570.

Roussel, J.R., Auty, D., Coops, N.C., Tompalski, P., Goodbody, T.R.H., Sánchez Meador, A., Bourdon, J.F., De Boissieu, F., Achim, A. 2020. lidR: An R package for analysis of Airborne Laser Scanning (ALS) data. *Remote Sensing of Environment* 251, 112061.

Wang, Y., Pyörälä, J., Liang, X., Lehtomäki, M., Kukko, A., Yu, X., Kaartinen, H., Hyyppä, J. 2019. In situ biomass estimation at tree and plot levels: What did data record and what did algorithms derive from terrestrial and aerial point clouds in boreal forest. *Remote Sensing of Environment* 232, 111309.

Wieser, M., Mandlburger, G., Hollaus, M., Otepka, J., Glira, P., Pfeifer, N. 2017. A case study of UAS-borne laser scanning for measurement of tree stem diameter. *Remote Sensing* 9(11), 1154.